Research Square

Preprints are preliminary reports that have not undergone peer review.
They should not be considered conclusive, used to inform clinical practice,
or referenced by the media as validated information.

Digital spatiotemporal landscaping of human chondrocyte differentiation during post-embryonic development

Hongwei Ouyang

hwoy@zju.edu.cn

Zhejiang University https://orcid.org/0000-0003-0627-2536

Dingchao Ying

Zhejiang University

Ya Wen

Zhejiang University

Jiansong Chen

The Children's Hospital, Zhejiang University School of Medicine

Heng Sun

Soochow University

Weiliang Wu

Zhejiang University

Heling Xue

Zhejiang University

Yiyang Yan

Zhejiang University https://orcid.org/0009-0002-6754-7476

Tian Qin

Soochow University

Chunmei Fan

Hangzhou Normal University

Bingbing Wu

Zhejiang University https://orcid.org/0000-0002-0250-104X

David Hay

University of Edinburgh https://orcid.org/0000-0002-7593-5973

Yishan Chen

Zhejiang University

Article

Keywords:

Posted Date: November 19th, 2026

DOI: https://doi.org/10.21203/rs.3.rs-11338464/v1

License: This work is licensed under a Creative Commons Attribution 4.0 International License.
Read Full License

Additional Declarations: There is **NO** Competing Interest.

Digital spatiotemporal landscaping of human chondrocyte differentiation during post-embryonic development

Dingchao Ying[1,2] †, Ya Wen[1,2] †, Jiansong Chen[3] †, Heng Sun[4], Weiliang Wu[3], Heling Xue[1,2], Yiyang Yan[1,2], Tian Qin[4], Chunmei Fan[5], Bingbing Wu[6], David C. Hay[1,7], Yishan Chen[1,2*], Hongwei Ouyang[1,2,8,9*]

1. Department of Sports Medicine of the Second Affiliated Hospital, and Zhejiang University-University of Edinburgh Institute (ZJE), and Liangzhu Laboratory, Zhejiang University School of Medicine, Hangzhou, 311100, China.
2. Dr. Li Dak Sum & Yip Yio Chin Center for Stem Cells and Regenerative Medicine, Zhejiang University School of Medicine, Hangzhou 310058, China.
3. Department of Orthopedic Surgery, The Children's Hospital, Zhejiang University School of Medicine, National Clinical Research Center for Child Health, Hangzhou, 310052 China.
4. Medical 3D Printing Center, Orthopedic Institute, Department of Orthopedic Surgery, The First Affiliated Hospital, School of Basic Medical Sciences, Interdisciplinary Innovation Center for Nanomedicine, MOE Key Laboratory of Geriatric Diseases and Immunology, Suzhou Medical College, Soochow University, Suzhou, Jiangsu 215000, China
5. Center of Frontier Science Research and Transformation, Hangzhou Normal University, Hangzhou, 311121, China
6. Department of Obstetrics and Gynecology, Center for Reproductive Medicine, the Fourth Affiliated Hospital of School of Medicine, and International School of Medicine, International Institutes of Medicine, Zhejiang University, Yiwu, 322000, China.
7. Centre for Regenerative Medicine, Institute for Regeneration and Repair, The University of Edinburgh, Edinburgh BioQuarter, Edinburgh EH16 4UU, UK.
8. Institute of Fundamental and Transdisciplinary Research, Zhejiang University, Hangzhou, 310058, China.
9. China Orthopedic Regenerative Medicine Group (CORMed), Hangzhou, China.

* Corresponding author. email: hwoy@zju.edu.cn; YishanChen@intl.zju.edu.cn.

† These authors contributed equally to this work.

Abstract

Chondrocyte differentiation governs skeletal formation, underpinning our understanding of human skeletal development and cartilage regenerative design. Existing human datasets are limited to early embryonic and late adult stages, leaving the critical post-conception week 9 to postnatal window poorly resolved. This gap obscures how compartmentalized osteochondral architectures are assembled from homogeneous mesenchymal condensates, and hinders digital predictive modeling of osteochondral biology and regeneration. Here, we comprehensively profiled human post-embryonic digits and identified prominent chondrocyte diversification from post-conception week 11 onwards. Integrating single-cell and spatial transcriptomics with in situ validation, we resolved osteochondral, perichondral, vascular, and hematopoietic subpopulations and characterized key transitional chondrocyte states, including naive, typical, hypertrophic, and fibrotic chondrocyte subsets. Our analyses revealed the emergence of *COL2A1*^{high} chondrocyte subpopulations, their cell-cell crosstalk, and their bifurcated developmental trajectories toward articular-surface and bone fates respectively. We mapped the spatiotemporal patterns of crucial progenitor cell biomarkers within the niche, including gremlin1 (GREM1), proteoglycan 4 (PRG4), and periostin (POSTN). Moreover, a rare *HLA-DRA*^{high} subpopulation was discovered. This subpopulation co-expressed chondrocyte markers and antigen-presenting cell signatures, representing a fundamental but undiscovered transitional state during cartilage-to-bone differentiation. We further demonstrated that our digital Post-Embryonic Chondrocyte Niche Atlas was a reliable reference for optimizing human cartilage organoid engineering. These advances have led to the identification of new transition states in chondrocyte developmental plasticity. In summary, these studies provide new fundamental knowledge for post-embryonic skeletal maturation, and a robust digital resource to advance chondrocyte-based research and future regenerative therapies.

Introduction

Textbooks categorize cartilage based on its histological and anatomical features, yet recent studies hint at additional chondrocyte subtypes [1-3]. In principle, chondrocyte phenotypes are not fixed, and abundant intermediate states arise particularly during development [4]. Programmed chondrocyte differentiation is central to vertebrate limb morphogenesis, supporting the formation of transient templates for skeleton, and generating articular cartilage for weight-bearing in joints [5]. These capacities stem from the intrinsic phenotypic plasticity of chondrocytes. Moreover, their plasticity holds key translational value for regenerative therapies in cartilage repair, which not only needs proliferative cell sources, but also precise differentiation of specialized cell subtypes, such as hyaline chondrocytes [6]. This phenotypic plasticity was maintained in human embryonic cartilage, but lost in adulthood, and current organoid systems cannot faithfully recapitulate the ability and programs [7]. Notably, with digital cellular profiling widespread, there is an urgent demand for continuous, high-resolution, cell-type-resolved datasets that capture real-world information. Models constructed without such data remain poorly compatible with in silico computational frameworks [8-10]. These underscores the critical need to characterize intermediate human chondrocyte subtypes and their regulatory cues, to provide natural references in developmental and regenerative-medicine studies.

Key events of chondrocyte differentiation during human development, include mesenchymal condensation at post-conception week (PCW) 5-6, and chondrocyte proliferation and hypertrophy from approximately PCW 6 onwards, followed by matrix mineralization from approximately PCW 7 onwards [11-13]. Concurrently, articular cavities form at PCW 7-8, and osteochondral complex maturation coordinates with perichondral niche remodeling [14,15]. Building upon previous knowledges, high-resolution documents of human embryonic limb development has been provided, uncovering chondrogenic progenitors (e.g. $SOX9^{low}COL2A1^{low}PRRX1^{high}$ osteochondral progenitors, $POSTN^{+}COL1A1^{+}PRRX1^{+}TWIST1^{+}$ chondrocyte progenitors) and master transcriptional regulators (SOX5/6/9, MAFF, NKX3-2) [13,16]. Nevertheless, critical gaps still exist. Current datasets are mostly restricted to human embryonic or adult tissues, leaving intermediate developmental phases poorly characterized [13,16,17]. It remains unclear how immature chondrocytes undergo fate diversification toward articular surfaces, stratified growth-plate zones or ossification centers in humans. The local molecular signals and niche crosstalk that govern

site-specific chondrocyte specialization therefore remain undiscovered. Although animal studies offer detailed mechanistic insights, interspecies differences still limit direct extrapolation to humans.

Digits constitute a cost-effective model for studying post-embryonic (post-PCW9) chondrocyte differentiation. Digits, fingers and toes, are limb-derived structures that execute advanced fine motor skills in humans. They share conserved developmental programs with long bones, including axial patterning, mesenchyme-cartilage-ossification cascades, and synovial-joint development [18]. Post-embryonic human digits (PCW9 to postnatal stages) attain advanced structural and functional maturation compared to embryonic tissues, offering biological insights into chondrocyte transient behaviors and their niche alterations [19,20]. Notably, post-embryonic digits harbor chondrocytes with both proliferation and differentiation abilities, positioned between uncommitted progenitors and terminally chondrocytes [21,22]. Such transitional cells constitute a valuable roadmap for graft construction, validating post-embryonic digits as an excellent model for human chondrocyte differentiation and cartilage organoid studies.

Here, we comprehensively phenotype chondrocyte development and differentiation bridging the unchartered gap between early-embryonic development and adult osteochondral biology. To resolve the critical time window, PCW9 to postnatal stages, we adopted a single-cell transcriptomics and spatial validation approach to map the diversity of collagen type II (COL2)-positive chondrocytes, their temporal emergence and their differentiation toward articular surfaces, hypertrophic cartilage and ossification centers. Our dataset defines spatiotemporally signaling mediating crosstalk between chondrocyte subpopulations and chondrocytes to their niche. We also validate the distribution of progenitor cells across epiphyseal cartilage, located at joint surfaces and perichondral tissues, and identify a previously undescribed chondrocyte subpopulation implicated critical to cartilage-to-bone transition. Finally, native in-vivo signatures from our work serves as an informative reference to benchmark organoid-derived cartilage phenotypes, providing phenotypic readouts for future cell-based regenerative therapies.

Results

Cellular diversity in the human post-embryonic digits

We performed single-cell RNA sequencing (scRNA-seq, Singleron GEXSCOPE platform) of digit tissues from 19 human donors (5 fetal digits, PCW11-25; 14 postnatal digits, donor age: 3 months-15 years old) (Fig. 1A and Table S1). All of the digits had already formed hinge joint structures. 129,561 cells passed quality control (Fig. S1), and were classified into 14 distinct clusters covering osteochondral tissue, peri-chondral connective tissue, vascular tissue and hematopoietic lineages (Fig. 1B and Table S2). In these clusters, 71.16% were enriched with typical cartilage biomarker *COL2A1*, and 14.32% expressed *COL1A1*, outlining the major subpopulations (Fig. 1C and 1D).

Six clusters highly expressed cartilage markers *COL2A1* and *COL9A1*, termed naïve chondrocytes (naïve chon), typical chondrocytes (typical chon), hypertrophic chondrocytes (hypertrophic chon), fibro chondrocytes (fibro chon), *SOX5*^{high} chondrocytes (*SOX5*^{high} chon) and *HLA-DRA*^{high} chondrocytes (*HLA-DRA*^{high} chon) (Fig. 1C-1F). Among them, naïve chon cluster was characterized by high expressions of skeletal progenitor cell markers *GREM1* (Gremlin1, GREM1) and *CPXM1*, and low expressions of bone developmental markers *PTH1R* and *OGN* [23-26] (Fig. 1C-1E). Typical chon were shown with a lower level of *GREM1* and a higher level of *PTH1R* (Fig. 1C-1E) compared to naïve chon. Hypertrophic chon and fibro chon both expressed a moderate level of *COL2A1* and *COL9A1*. The former were enriched with *COL1A1*, *PTH1R*, *PDPN* and *COL10A1*, and the latter were marked by *CLU*, *POSTN*, *OGN*, and *PRG4* (Fig. 1C-1E) [27-29]. The other two minor chondrocyte clusters *SOX5*^{high} chon and *HLA-DRA*^{high} chon, were characterized with chondrogenic markers SOX5 and major histocompatibility complex (MHC)-relevant gene *HLA-DRA*, respectively [30,31] (Fig. 1C-1E).

We also uncovered eight subpopulations with low *COL2A1* expression, including *COL1A1*^{high} perichondral cells (*COL1A1*^{high} peri-chon) expressing perichondrium / periosteum marker *POSTN*; *PRG4*^{high} cells with low *COL1A1* and minimal *COL2A1* expression; endothelial cells featured by *PECAM1* and *EMCN* [32]; vascular smooth muscle cells (VSMC) enriched with *RGS5*, *ACTA2*, and *TAGLN* [33]; hematopoietic cells expressing *PTPRC* and *SRGN* [34,35]; lymphocytes expressing *IGHM* and *CD74*, mast cells with *TPSB2* and *TPSAB1* [36,37]; and erythroid cells marked with *HBB* and *GYPC* [38] (Fig. 1B and 1D).

Osteochondral tissue forms the framework of digits, surrounded by soft connective tissues that link hinge-type interphalangeal joints. The formation of ossification centers

also represents vascular ingrowth and the formation of hematopoietic lineages [39]. On this basis, immuno-staining identified the clusters' location (Fig. 1G). Collagen type II (COL2) demarcated a sharp boundary of articular cartilage, supposed to be where the six *COL2A1*^{high} chondrocyte clusters (naïve chon, typical chon, hypertrophic chon, fibro chon, *SOX5*^{high} chon and *HLA-DRA*^{high} chon) reside (Fig. 1B and 1G). Hypertrophy marker *PDPN* (expressed in hypertrophic chon) was detected in the hypertrophic zone (HZ) of growth plate, validating the zonal cartilage differentiation during post-embryonic stages (Fig. 1G). Collagen type I (COL1) and perichondrium / periosteum marker *POSTN* (expressed in *COL1A1*^{high} peri-chon) were also displayed in peri-chondral soft tissues (Fig. 1H). Markers including CD31(endothelial cells), ACTA2 (VSMC), HBB (erythroid cells), IGHM (lymphocytes), TPSAB (mast cells) and CD45 (hematopoietic cells) were detected within peri-chondral connective tissues and the medullary cavity (Fig. 1I and 1J).

We identified cell diversity in human post-embryonic digits. Within the well-defined COL2-positive area, chondrocyte transitional subpopulations could be distinguished, highlighting the complexity of chondrocyte phenotypes during post-embryonic development.

Emergence of *COL2A1*^{high} chondrocytes and niche remodeling programs in post-embryonic stages

To visualize developmental features, we integrated our data with a key published human embryonic limb dataset (E-MTAB-8813), which contained distal and middle limb samples at PCW5–6, when early cartilaginous anlage and interzone had just formed [13]. The integrated analysis included 191,873 single cells, and resolved 15 clusters found both in embryonic limbs and post-embryonic digits (Fig. 2A-2C). The shared clusters were naïve chon, typical chon, hypertrophic chon, fibro chon, *COL1A1*^{high} cells, *PRG4*^{high} cells, *SOX5*^{high} chon, proliferating cells, *EMX2*^{high} cells, endothelial cells, VSMC, erythrocytes, lymphocytes and hematopoietic cells, validating the similarity in their tissue origin (Fig. S2A).

In the post-embryonic tissues, we observed an evident enrichment of *COL2A1*^{high} chondrocyte subpopulations (naïve, typical, hypertrophic and fibro chon), compared with embryonic samples (55.40% *vs* 20.25%, post-embryonic *vs* embryonic), correlating to enhanced cartilage maturation at post-embryonic stage [40]. Genes and gene ontology (GO) terms related to cartilage extracellular matrix (ECM) (*COL2A1*, *COMP*,

ACAN, *COL9A1*) were generally enriched in post-embryonic samples (Fig. 2D and 2E). On the contrary, *COL1A1*^{high} clusters (*COL1A1*^{high} cells and *PRG4*^{high} cells) were less abundant in post-embryonic samples (19.60% *vs* 42.85%, post-embryonic *vs* embryonic) (Fig. 2C). Even within *COL1A1*^{high} subpopulations, higher expressions of differentiation-associated genes (*COL3A1*, *OGN*, *PRG4*) could be observed in post-embryonic samples (Fig. 2F), further validating their advanced developmental maturation (Fig. 1A).

We also compared the developmental maturity between fetal and postnatal samples within the post-embryonic cohort. Postnatal digits exhibited significantly increased length of phalanxes in both distal and proximal parts, and increased formation of primary and secondary ossification centers (POC, SOC) (Fig. 2G-2I) [41,42]. *SOX5*^{high} chon declined in the postnatal samples, whereas *COL1A1*^{high} peri-chon, endothelial cells and VSMC showed an increase in cluster proportion (Fig. 2J, S4B and S4C), suggesting the growth of peri-chondral connective tissue and vascular tissue in postnatal digits. Matrix-remodeling genes, including *MMP12*, *MMP3* and *SERPINA5*, were enriched in all postnatal cartilage clusters (naïve chon, typical chon, hypertrophic chon, fibro chon) (Fig. 2K and 2L). To avoid the mismatch between development stage and donor age, the post-embryonic digits were also classified based on anatomical structures: stage 1 (short fetal digits); stage 2 (postnatal digits with incompletely developed POCs); stage 3 (postnatal digits with formed medullary cavities without mature SOCs); stage 4 (long postnatal digits with developed structures) (Fig. 2G and Table S3) [39,43,44]. The changes in their cluster proportions mirrored the fetus-vs-postnatal trends above, with perichondral lineages increasing dramatically at stage 4 (donor age 11 to 15y).

Collectively, the post-embryonic digits exhibited enhanced maturation of cartilage compared to the embryonic limbs, indicated by a shift from *COL1A1*- dominant tissues to *COL2A1*-dominant ones. When comparing the temporal features among post-embryonic samples, we exhibited structural maturation of phalanges, enhanced ECM remodeling in chondrocytes, and increased accumulation of peri-chondral connective tissues in postnatal relative to fetal digits.

Dynamical programs of chondrocyte fate commitment and niche crosstalk

In the embryonic to post-embryonic comparison, post-embryonic samples showed prominent chondrocyte differentiation. It motivated us to look into their interactive signaling that drove the developmental programs.

With RNA velocity analysis (scVelo, v0.3.2), we uncovered a potential bifurcated trajectory of chondrocyte phenotype specification (Fig. 3A and 3B). The two branches both started with naïve chon, given that they were marked by stem cell or progenitor cells genes, representing the least differentiated state. This was also consistent with their minor proportion of at stage 4 (Fig. S3E). One branch was as a cartilage-to-bone trajectory, deriving from naïve chon to typical chon, and ending at hypertrophic chon; the other was a cartilage-to-articular surface branch, from naïve chon to fibro chon, and was highly associated with *COL1A1*^{high} peri-chon (Fig. 3A). Monocle 3 analysis (v1.3.4) showed that the cartilage-to-bone trajectory was accompanied by upregulation of *COL10A1*, *IBSP*, and *SPP1*, and the fibrogenic trajectory was marked by upregulation of *ABI3BP*, *POSTN*, and *PRG4* (Fig. S4A and S4B).

Regulon analysis (pySCENIC, v0.12.1) supported their identity associations (Fig. S5). Naïve chon, typical chon and fibro chon were generally enriched with regulons of SRY-box transcription factor 9 (*SOX9*), the typical transcription factor (TF) for cartilage lineage [45], whereas they also obtained their specific regulon features. Naive chon were also marked by *LHX9* and *NFATC2* regulons, correlated to early limb development and cartilage homeostasis [46,47]. Typical chon retained *NKX3.2*, *FOXO4*, and *RUNX3* regulons, more correlated with cartilage maturation [48-50]. Relatively, fibro chon, hypertrophic chon, *COL1A1*^{high} peri-chon and *PRG4*^{high} cells showed less similarities with naïve chon and typical chon (Fig. S5), and were enriched with their specified regulons (hypertrophic chon: *RARB* and *DLX5,* for chondrocyte hypertrophy [51,52]; *HLA-DRA*^{high} chon: *E2F1*, *E2F7* and *E2F8*, involved in cell proliferation and endochondral ossification [53,54] ; fibro chon: *GLI3* and *ERG*, related to articular surface formation [55-57]; *COL1A1*^{high} peri-chon: *NR2F2* that regulates mesenchyme tissue) [58,59]. The data indicate that naïve and typical chon are close to authentic cartilage lineage, while the others show phenotypic shifts on the cartilage-to-bone or cartilage-to-articular surface trajectories.

In terms of regulatory signaling between these clusters, Cell Chat analysis demonstrated a more chondrocyte-centric interactive pattern among naïve, typical and fibro chon at postnatal stages (stage 2-4) relative to those observed at fetal stage (stage 1) [60] (Fig. 3C). ECM-related pathways (COLLAGEN, FN1 and TENASCIN) were commonly

enriched across 4 stages, highlighting the essence of matrix remodeling through post-embryonic development. The diversity of communication signaling pathways were shown to increase alongside development (Fig. 3D). Canonical osteochondrogenic signals, including Transforming Growth Factor beta (TGF-β) and Bone Morphogenetic Protein (BMP) pathways, were enriched at stage 2 and 3 as both outgoing and incoming signals in typical chon, and TGF-β alone was enriched at stage 4 (as outgoing signal in *HLA-DRA*^{high} chon; as incoming signals in typical and naïve chon) (Fig. 3D and S6). Adhesion- and migration-related pathways, including ITGB2, PTPRM, and EPHA, were highlighted at stage 4 in *HLA-DRA*^{high} chon, indicating the association with cell migration or angiogenesis for bone development [61-63] (Fig. 3D and S6).

Together, we displayed differentiation trajectories (cartilage-to-bone and cartilage-to-articular surface) among the major clusters residing in and around cartilage. The data revealed timely fluctuations in of chondrocyte subpopulations and signaling activity during chondrocyte differentiation.

Spatiotemporal presence of putative progenitor cells

We next focused on representative functionally pivotal subpopulations in cartilage development and repair, and analyzed their stage-dependent spatial changes.

Naïve chon, presenting the least differentiated cluster with chondrocyte identity, highly expressed *GREM1* (Fig.S7A and S7B). The gene encodes the secreted protein gremlin 1 (GREM1), a BMP antagonist that maintains cell undifferentiated state and was recognized as a skeletal stem cell label in mice and humans reportedly [64-66]. In our data, naïve chon's markers *GREM1*, *DLK1*, *CYTL1* and *CPXM1* were down-regulated from stage 1 to 4 (Fig. S6C). Immuno-staining revealed that GREM1 and Carboxypeptidase X, M14 Family Member 1 (CPXM1) were broadly expressed throughout the epiphyseal cartilage (GREM1: 91.77% of cartilage area; CPXM1: 91.87% of cartilage area), while the overall expression of GREM1 decreased with development progression (Fig. S7D and S7E). Consistently, in spatial transcriptomics analysis (GeoMX digital spatial profiler (DSP)), chondrocytes at GREM1^{high} regions were detected with less osteochondral matrix genes (*COL2A1*, *ACAN*, *SPARC*, and *CCN2*) and GO terms (ossification, cartilage condensation and ECM organization), compared to those at GREM1^{low} cartilage regions (Fig. S7F and Table S4). These data indicated that GREM1

preferentially marked chondrocytes at early developmental stages. To validate their function, we isolated chondrocytes from stage 1-2 postnatal digits, and displayed that they were capable of single-cell colony formation, which positively expressed GREM1 (Fig. S7G). And they also possessed the ability of multi-lineage differentiation (Fig. S7H). GREM1 is a well-known molecule in cartilage development and repair [67-69]. Extending previous studies, we validated the existence of *GREM1*^{high} chondrocytes in the critical intermediate developmental window, which were supposed to preserve the progenitor properties while beginning to acquire chondrocyte identity.

In fibrogenic trajectory, fibro chon and *PRG4*^{high} cells were both featured by *PRG4* (Proteoglycan 4, lubricin) (Fig. 1E, 3A, S8A and S8B). The marker represents superficial chondrocyte progenitors at joint surfaces, and is essential for cartilage niche maintenance [70]. In our samples, proteoglycan 4 (PRG4) was widely stained in epiphyseal cartilage in fetal stage, but gradually restricted to articular surfaces in postnatal joints (Fig. S8D). In spatial transcriptomics, PRG4^{high} regions within cartilage were enriched with GO terms of Wnt signaling, stress-responses, and G1/S cell-cycle transition, in contrast to PRG4^{low} ones with typical chon features, consistently with previous studies of Prg4+ progenitors [71] (Fig. S9A and Table S4). We adopted ligand–receptor analysis of scRNA-seq data and found that CD99–CD99 and COL1-(ITGA10+ITGB1), which regulated cell self-renewal and cell-matrix adhesion respectively, were top signaling pairs between *PRG4*^{high} cells and the other subpopulations (Fig. S10B and S10C), indicating their role in supporting cartilage growth and niche homeostasis [72,73].

Another fibrogenic biomarker, periostin (POSTN), was captured in both fibro chon and *COL1A1*^{high} peri-chon (Fig.1E, S9C and S9D), consistent with previous documents of Postn+ progenitors in perichondrium and periosteum [26,74]. In perichondrium and periosteum, POSTN expression was also in a broad-to-restricted trend alongside development, and diminished at stage 4 (Fig. S9D). This matched the findings that Postn+ progenitors declined with age [75]. Differently, GREM1 and periosteum marker OGN (Osteoglycin) were not shown with location-restriction in perichondral connective tissue (Fig. S8D and S9D).

Together, we validated the existence of progenitor subpopulations, the roles of which have been well documented previously. GREM1 was widely expressed across post-embryonic epiphyseal cartilage, yet its expression declined with development. PRG4 and POSTN became restricted to joint surfaces or perichondrium / periosteum as

development proceeded. Given that they are crucial matrix proteins in regulating progenitors' niche, their expression shifts may be linked to the age-related exhaustion of stem cell pool, and cell-fate-coupled niche remodeling by ECM-degrading enzymes in postnatal digits.

Discovery of *HLA-DRA*^{high} chon, a new chondrocyte subpopulation with early ossified phenotype

Besides fibrogenic trajectory, the other essential branch corresponds to cartilage-to-bone differentiation (Fig. 4A). The major clusters typical chon and hypertrophic chon were characterized by ECM remodeling genes including *CNMD*, *MATN3*, *SNORC*, *CCN2*, *FGFBP2* and *PDPN* (Fig. S10A and S10B). The representative gene *PDPN* encoded protein PDPN (podoplanin), positively detected in 82.69% of hypertrophic regions (POCs, SOCs, hypertrophic zones of growth plate, deep layers of articular cartilage) across all post-embryonic samples (Fig. 4B-4D). Its positive detection ratios were 88.89% in stage 1 and 100% across stages 2 to 4, reaching 66.67% in POCs and 100% in SOCs (Fig. 4C, 4D and S11A). These was consistent with its correlation with endochondral ossification [76].

Notably, we identified a rare cluster (3.79% of digit subpopulations in scRNA-seq data), which co-expressed *COL2A1* and *HLA-DRA* (Fig. 1E, 1F and S11B). *HLA-DRA* encodes HLA-DR receptor, an MHC Class II protein constitutively expressed in antigen-presenting cells (APCs) [77]. Cartilage is generally regarded as immunologically quiescent and lacks canonical immune markers [78]. However, we observed a clear expression of HLA-DR within epiphyseal cartilage, positively stained with COL2 (Fig. 4E and 4F). HLA-DR could be positively stained in 40.98% of hypertrophic cartilage regions, and the positive ratios were 100%, 40%, 71.43% and 0% at stage 1 to 4 respectively (Fig. 4C and S11A). It could also be positively detected in deep and calcified zones of adult articular cartilage (Fig. 11C and 11D).

As HLA-DR was detected across multiple hypertrophic sites at different stages, we reasoned that this signature did not mark discrete anatomical compartments but captured a transitional cell state during chondrocyte osteogenic differentiation. To validate HLA-DR's presence during cartilage-to-bone transition, we generated chondrocyte organoids under step-wise induction that produced a central-to-peripheral cartilage-to-bone gradient (Fig. 4G-4I). HLA-DR was seen in areas between the cartilage core and the most osteogenic layer (alkaline phosphatase-positive) (Fig. 4H

and 4I). Consistently, in human post-embryonic epiphyseal cartilage that just initiated SOC development, we conducted three-dimensional immunostaining of HLA-DR and observed that HLA-DR coincided with the presence of the cavity at the core of epiphyseal cartilage, corresponding to pre-SOC sites that had not yet undergone full vascularization (Fig. S12A and S12B). Together, the results indicated that HLA-DR stood for chondrocytes with hypertrophic phenotype, at an intermediate stage during cartilage-to-bone development.

The essentiality of HLA-DR expression during chondrocyte osteogenesis was validated in a chondrocyte osteogenic model. We demonstrated that siRNA knockdown of HLA-DR significantly reduced the alkaline phosphatase intensity in human post-embryonic chondrocytes after an osteogenic induction in vitro (Fig. 4J). In parallel, treatment of an HLA-DR antibody that block HLA-DR's interaction with other molecules during induction, also significantly attenuated osteogenic differentiation (Fig. 4K).

DSP demonstrated that chondrocytes in HLA-DR^{high} pre-ossification centers, were enriched with genes and GO terms governing the emission and reception of osteogenic signaling (*BMP8A* and *PTH1R*; GO terms: ossification, BMP signaling, and cell migration) (Fig.4K, 4M, S13A and Table S4). It raises the possibility that *HLA-DRA^{high}* chon participate in the regulation of cartilage ECM remodeling. As a MHC class II molecule, HLA-DR presents exogenous antigenic peptides in APCs, which further amplify immune responses [79]. Likewise, chondrocytes induced matrix degradation in hypertrophic regions, leading to accumulation of immunogenic protein fragments [80,81]. HLA-DR on chondrocyte cell surfaces may present matrix-derived fragments or interact with other niche molecules, which facilitates mineralization and vascular invasion (Fig. S13B). Cell Chat analysis predicted that these cells transmitted PTN signaling to neighboring cells (Fig. 4N). *PTN* encodes pleiotrophin (PTN), a heparin-binding cytokine that induces osteogenesis [82]. Immunostaining validated that HLA-DR and PTN proteins were partially co-localized (37.52% of HLA-DR^{high} POCs and 77.57% of HLA-DR^{high} SOCs overlapped with PTN detections), whereas HLA-DR was closer to the hypertrophic zones or pre-ossification centers, with PTN accumulating at the surrounding less osteogenic sites (Fig. 4O, Fig. S13C-S13E). Besides spatial gradient, the hypertrophic markers *PTN*, *HLA-DRA* and *PDPN* exhibited stage-dependent expression patterns, with peak expression at stage 1, 2 and 3 respectively (Fig. S13F), demonstrating the sequential rises and falls of niche signaling during intermediate stage of endochondral ossification.

Together, we examined the stage-dependent spatial features of osteogenic clusters, and uncovered a new subpopulation termed *HLA-DRA*^{high} chon. The data suggest that chondrocytes undergoing cartilage-to-bone transition, actively regulate their surface and secreted proteins to mediate spatially restricted, immune-relevant programmed ECM remodeling in prior to vascularization. The findings may extend existing knowledge of endochondral ossification and remodeling.

The digital Post-Embryonic Chondrocyte Niche Atlas (PECNA), a reference to guide organoid engineering

Our data demonstrate the complexity of chondrocyte and niche phenotype, necessitating a more detailed cell characterization in cartilage biological and engineering studies [83,84]. It highlights the necessity of providing well-matched, continuous and high-resolution digital cellular information for optimizing real-world cell culture. Previously, we established a human cartilage organoid system with customized culture medium, the function of which has been validated in previous animal studies [85]. Building on this system, we demonstrated that our data, as a human Post-Embryonic Chondrocyte Niche Atlas (PECNA), could serve as a digital reference for evaluating engineered cartilage and guiding optimization of chondrocyte culture.

Based on our previous study, postnatal chondrocytes were isolated (Table S5), induced into organoids under a customized condition (CC), and collected on two critical days (Day 6 and 27). The primary cells, Day-6 cells, and Day-27 cells were named P0, CC1 and CC2 respectively. Control chondrocytes from identical sources, cultured in conventional medium, and collected on matched time points, were named TC1 and TC2 (typical condition, TC) respectively (Fig. 6A).

We then harvested 57,139 cells for scRNA-seq of P0, CC1, CC2, TC1, TC2 groups, and integrated them with our PECNA dataset. The in vivo and in vitro datasets exhibited highly overlapping cell compositions, confirming that the organoids recapitulated native tissue features (Fig. 5B and 5C, S14A-S14C). Some subtle differences were shown to reflect culture-induced alterations in cell subpopulations, including the absence of endothelial cells and the accumulation of *MT1*^{high} chon, an in vitro-specific subpopulation marked by metallothionein genes *MT1X*, *MT1G* and *MT1E* (Fig. 5B and 5C, S14A-S14C). These changes suggest that the organoid culture yields more purified chondrogenic tissue, but induces metabolic remodeling in cell expansion[86].

PECNA could provide marker panels to assess the developmental status of cultured organoids in vitro. The marker *GREM1* was used to identify undifferentiated stages, which was highlighted in P0, CC1 and TC1, but down-regulated in CC2 and TC2 (Fig. 5D). Typical chon biomarkers (*SOX9*, *COL2A1*, *COL9A3*, *CNMD* and *MATN3*) for chondrocyte differentiated phenotype were enriched in P0 and CC2 rather than TC2, whereas fibro chon genes (*PRG4* and *POSTN*) were shown in TC2, indicating that our customized culture induced a superior native-like phenotype of hyaline cartilage (Fig. 5D). *HLA-DRA* was minimally expressed in all in vitro groups (Fig. 5D), matching the published results that polydactyl chondrocytes exhibited low immunogenicity [87], suggesting that HLA-DR's expression in chondrocytes may depend on inductive cues under osteogenic microenvironments.

Phenotypic profiling further revealed early-phase cellular reprogramming under customized induction. CC1 exhibited marked depletion of hypertrophic chon (18.19% in TC1 vs 9.01% in CC1) alongside substantial expansion of a *COL1A1*^{high} subpopulation compared to TC1 (2.18% in TCs vs 23.84% in CC1) (Fig. 5E). CC1 *COL1A1*^{high} cells exhibited increased stem-cell/progenitor- and adhesion-associated genes (*PRRX1*, *SOX4*, *THY1*, *NT5E*, *CD44*, *ITGB1, FN1*) [88-91], but TC1 showed elevation of cartilage-matrix genes (Fig. 5F). GO terms linked to ossification and ECM organization were enriched in both, whereas CC1 displayed additional enrichment for wound-healing-related biological processes (Fig. S14D).

Furthermore, the profiling revealed subtle subpopulation differences that cannot be resolved by conventional bulk ECM markers such as COL1. Based on PECNA, we found organoid-derived *COL1A1*^{high} cells were transcriptionally distinct from *COL1A1*^{high} peri-chon in vivo. Organoid *COL1A1*^{high} cells demonstrated elevated expression of mitochondrial rRNA genes (*MT-RNR1/2*), ribosomal-protein-coding genes (*RPL7*, *RPL21*, *RPS26*), proliferation / adhesion-related genes (*CYR61*, *FN1*, *CHI3L1*, *H3F3B*) [92-95], consistently with the enriched GO terms relevant to energy metabolism, and wound healing (Fig. 5G and 5H). This population also up-regulated cartilage progenitor genes, including *PRRX1*, *PDGFRA*, *FOXP1*, *THY1* and *NT5E* (Fig. 5I) [88,96]. *COL1A1*^{high} peri-chon preferentially expressed *ECRG4*, *OGN*, *COL14A1*, *COL3A1* and *CLU*, consistent with perichondral connective tissue identity (Fig. 1E and 5I). These finely explained the function of stemness-maintaining components in our customized culture medium, which might play a role in cell phenotype reprogramming to gain progenitor features in early-stage expandable organoids. These findings explain

why our CC system enables the generation of intact and functional organoids (Fig. S14E), and further provide actionable clues for future medium optimization.

Collectively, the human digital PECNA serves as a blueprint for chondrocyte expansion. It enables identification of new chondrocyte phenotypes which correspond to key developmental intermediates, high-resolution tracing of cell fates during in vitro induction, the detection of aberrant non-native subpopulations, and allows broad ranging comparison between different culture protocols. This resource facilitates targeted, precise optimization of current cartilage graft culture systems, and provides more finely resolved trajectories of chondrocyte differentiation for constructing digital cellular and tissue models.

Discussion

We present a dataset that captures intermediate developmental phenotypes of human chondrocytes, thereby filling a knowledge gap between embryonic and mature stages. Compared to embryonic limbs, our samples show pronounced enrichment of *COL2A1*^{high} chondrocyte subpopulations bearing differentiated phenotypes, alongside anatomical structural maturation. Although COL2 spatially demarcates cartilage from perichondral tissues, the rich transitional subpopulations within cartilage, for example, naïve, typical, hypertrophic, fibro chon, do not exhibit discrete boundaries at the fetal stage. These chondrocytes gradually specify two fate branches toward articular surface or ossification specialization at postnatal stages. Our analysis indicates that the presence of these heterogeneous intermediate subpopulations coincides with increased complexity of signaling cascades at postnatal stage 3 and 4, involving osteogenic and angiogenic factors that drive further development progression. It reflects the emergence of chondrocyte diversification and key intermediate states during post-embryonic stages.

Along both trajectories of chondrocyte differentiation, ECM remodeling becomes a central program. This is driven by degradation of pre-existing matrix (for instance, by matrix metalloproteinases (MMPs)) and spatiotemporally constrained secretion of different proteins. We identified three distinct expression patterns for key niche molecules. Firstly, GREM1, which maintains cell undifferentiated states across the epiphysis, is down-regulated over developmental stages without evident shifts in spatial restriction. Secondly, PRG4 and POSTN, sustain homeostasis at joint surfaces and perichondrium / periosteum, exhibit progressive spatial restriction as development proceeds. These patterns indicate that certain populations function as widely distributed progenitor reservoirs, while others depend on site-specific anatomical architecture and local microenvironmental cues. Thirdly, hypertrophic and *HLA-DRA*^{high} chon are not broadly distributed at any stages in our samples, but they tightly correlate with cartilage hypertrophy and endochondral ossification, coinciding with vascular and cell migratory signaling. *HLA-DRA*^{high} chon represents a rare subpopulation expressing HLA class II receptor conventionally restricted to APCs.

Cartilage has long been considered devoid of immune markers and the scarcity of prior reports on chondrocyte HLA-DR expression suggests that its induction requires specific in vivo or experimental microenvironmental cues. Functional validations confirm that HLA-DR supports pre-hypertrophic chondrocyte priming toward osteogenic

commitment (Fig. 4, S11-S13). These unexpected observations indicate that chondrocytes actively remodel cell-surface interactions to enable osteogenic differentiation. Such remodeling may be triggered by the accumulation of immunogenic matrix fragments after ECM breakdown and may further promote inflammatory signaling or vascular invasion. Furthermore, the graded distribution of PTN and HLA-DR points to amplification of local osteogenic cascades into adjacent tissue, establishing the cartilage-to-bone transition. Because HLA-DR is detectable in hypertrophic regions across fetal, infant and even adult cartilage (Fig. 4, S11), these findings may uncover a general mechanism whereby chondrocytes propagate osteogenic programs by reshaping cell-niche interactions.

Beyond insights into developmental biology, the blueprint we generated provides a reference and standardized guide to engineering tissue grafts. In particular, cartilage repair research urgently requires cell resources that retain regenerative potential while preserving chondrocyte identity. However, existing datasets lacked information on intermediate-state chondrocytes, constraining of knowledge and modeling, including the development of advanced computational models. Complementing previously published datasets, we established a valuable resource bridging wet-lab experiments and digital modelling. Its applications include benchmarking cultured organoids against native tissue reference, identifying whether intermediate subpopulations are recapitulated or whether culture-specific cell states emerge, and tracing trajectories of cellular reprogramming during induction. With this resource, integrated analysis with prior datasets enables comparison of chondrocyte states across developmental stages, offering foundational data that support the future development of artificial intelligence (AI)-powered virtual models and helping fill the gap between real-world biological measurements and in silico cell simulations.

We also acknowledge that this study carries several limitations. The atlas was built partly using polydactyl digits, which are experimentally accessible yet may exhibit developmental discordance or delay relative to chronological donor age. To mitigate this bias, we selected specimens with intact joint architecture and staged samples using anatomical criteria (phalange length, POCs, SOCs) rather than donor age. Their subpopulation profiles align with limb and fetal tissue datasets and capture more mature developmental structures and cell states than many existing resources. The key results are consistent across the fetal-to-postnatal timeline and are not confined to polydactyl samples, thereby strengthening the credibility of our observations. Given the limited

accessibility of healthy human tissues, the dataset remains highly valuable for human developmental biology. Furthermore, cell clusters were characterized exclusively in fixed tissue without in vivo lineage tracing. We inferred biological functions by integrating prior literature and validated the role of key molecules in primary human chondrocyte models. Despite interspecies divergence, functional assays in mouse models may yield further mechanistic insights.

In summary, this study delivers a new cellular and spatial atlas of human post-embryonic digits, revealing the phenotypic diversity of chondrocytes and the ECM-associated programs that govern cartilage and bone maturation during development. This in vivo reference further establishes a framework for evaluating engineered cartilage and informing cartilage regeneration strategies.

Method

Human tissue collection and ethics

Human digit tissues were obtained from two sources. Postnatal digit tissues were collected from pediatric patients undergoing corrective surgery for polydactyly at the Children's Hospital, Zhejiang University School of Medicine (Hangzhou, China). A total of 22 postnatal samples from donors aged 3 months to 15 years were included, and only well-formed digits containing intact cartilage, bone, and joint structures were used. Fetal digit tissues were obtained from the Fourth Affiliated Hospital of Zhejiang University School of Medicine following elective termination of pregnancy with written informed consent. None of the donors had a known history of genetic disorders other than polydactyly. Gestational age was estimated based on the last menstrual period (LMP) and converted to post-conception weeks (PCW) by subtracting approximately two weeks. Five fetal donors, estimated to correspond to PCW10–25, were included.

All procedures involving human participants were conducted in accordance with the Declaration of Helsinki. Collection and use of postnatal polydactyly tissues were approved by the Institutional Review Board of the Children's Hospital, Zhejiang University School of Medicine (Approval No. 2020-IRB-077), and fetal tissue collection was approved by the Institutional Review Board of the Fourth Affiliated Hospital of Zhejiang University School of Medicine (Approval No. K2021065). Written informed consent was obtained from the parents or legal guardians of pediatric donors and from the pregnant individual before fetal tissue collection.

Tissue processing and scRNA-seq data generation

Except for specimens allocated to three-dimensional reconstruction, each postnatal digit was bisected along the sagittal plane. One half was used for scRNA-seq or GeoMx Digital Spatial Profiling (DSP), and the other half was reserved for histological and immunostaining analyses. For fetal donors, multiple digits were collected per donor. The thumb was used for scRNA-seq and the remaining digits for histological and immunostaining analyses.

For single-cell dissociation, dissected tissues were minced and digested at 37 °C for approximately 4 h in an enzyme mixture containing dispase (3 mg/mL; Sigma-Aldrich, D4693) and collagenase types I and II (3 mg/mL each; Gibco). Cell suspensions were filtered through a 40-μm strainer and processed for library preparation. Postnatal samples were pooled in pairs for library construction and subsequently demultiplexed

using Souporcell. Single-cell capture, reverse transcription, cDNA amplification and library construction were performed using the GEXSCOPE workflow (Singleron). Libraries were sequenced on an Illumina platform with paired-end 150-bp reads (PE150).

scRNA-seq data processing, integration and clustering

Raw FASTQ files were processed using CeleScope (v1.10.0) (https://github.com/singleron-RD/CeleScope) with alignment to the human reference genome (GRCh38) to generate gene-by-cell count matrices. Count matrices were imported into Seurat (v4.4.0) [97] for quality control and downstream analysis. Cells with fewer than 200 detected genes, fewer than 500 UMIs, or more than 15% mitochondrial transcripts were excluded. Putative doublets were removed using DoubletFinder (v2.0.4) [98] with an expected doublet rate of 5%.

Pooled postnatal libraries were demultiplexed using Souporcell (v2.4) [99] based on single-nucleotide polymorphism (SNP) profiles and cells with ambiguous donor assignments were excluded.

Datasets were integrated in Seurat (v4.4.0) using the anchor-based canonical correlation analysis (CCA) workflow. For each sample, data were normalized and 2,000 highly variable genes were identified. Integration anchors were computed across samples to generate an integrated expression matrix.

Clustering and dimensionality reduction

The integrated data were scaled and subjected to principal component analysis (PCA). The top 20 principal components were used to construct a shared nearest-neighbor graph for Louvain clustering at a resolution of 0.5. UMAP was used for visualization. Cluster marker genes were identified in Seurat by differential expression analysis and used to annotate cell populations based on established lineage markers and canonical gene expression patterns.

Differential gene expression analysis and Gene Ontology analysis

Cluster marker genes were identified using the FindAllMarkers function in Seurat with the Wilcoxon rank-sum test. Genes detected in at least 25% of cells in either cluster and with a log fold change greater than 0.25 were retained.

For comparisons between experimental groups, counts were aggregated for each sample and cluster combination to generate pseudo-bulk profiles and analyzed using DESeq2 (v1.46.0). Genes with |log2FoldChange| > 1 and adjusted $P < 0.05$ were considered differentially expressed.

Gene ontology (GO) analysis was performed in R (v4.4.0) using clusterProfiler (v4.14.4) and org.Hs.eg.db (v3.20.0). Multiple-testing correction was performed using the Benjamini–Hochberg method, and terms with adjusted $P < 0.05$ were considered significant. Redundant terms were reduced using simplify() with a similarity cutoff of 0.7.

Cell–cell interaction analysis

Cell–cell communication analysis was performed using CellPhoneDB (v4.0.0) [100] and CellChat (v1.6.1) [101]. CellPhoneDB was used to assess interactions between cell populations. CellChat was used with CellChatDB.human to infer specific ligand–receptor interactions and signaling patterns across cell populations.

Trajectory inference and RNA velocity

Pseudotime analysis was performed using Monocle 3 (v1.3.4) [102]. Early progenitor populations were specified as trajectory roots, and cells were ordered along pseudotime. RNA velocity analysis was performed using velocyto (v0.17.17) [103] and scVelo (v0.3.2; Python 3.8.3) [104]. Aligned BAM files were converted to loom files containing spliced and unspliced count matrices for velocity estimation.

Transcription factor regulatory network analysis

Transcription factor (TF) regulatory network analysis was performed using pySCENIC (v0.12.1) [105]. To reduce computational burden, 2,000 cells were randomly sampled from each chondrocyte subpopulation for analysis. Raw count matrices were analyzed using the standard pySCENIC workflow, including gene regulatory network inference, cisTarget-based TF target enrichment, and AUCell-based regulon activity scoring. Regulon activity and network outputs were further analyzed in R using SCopeLoomR (v0.13.0), AUCell (v1.28.0), and SCENIC (v1.3.1).

Integration with comparative datasets

For comparative analyses, two additional single-cell datasets were included. For embryonic comparison, a published human embryonic limb dataset was obtained from BioStudies under accession E-MTAB-8813 (https://www.ebi.ac.uk/biostudies/arrayexpress/studies/E-MTAB-8813). Samples from distal and middle forelimb and hindlimb regions at PCW5.6 and PCW6.1 were included (WSSS_THYst9384953, WSSS_THYst9384954, WSSS_THYst9384956, WSSS_THYst9384957, WSSS_THYst8796438, WSSS_THYst8796439, WSSS_THYst8796441, and WSSS_THYst8796442). For in vitro comparison, an in-house cartilage organoid dataset was generated from freshly isolated polydactyly

chondrocytes (P0) and from organoids cultured under customized serum-free (CC1, CC2) or conventional serum-containing (TC1, TC2) conditions.

For embryonic integration, data were integrated using scVI [106] with dataset origin specified as the batch variable, followed by BBKNN [107] graph construction in the latent space. For in vitro integration, data were integrated in Seurat using the CCA-based workflow described above.

Digital spatial profiling

Cartilage specimens were processed for GeoMx Digital Spatial Profiling (DSP) using the GeoMx Human Whole Transcriptome Atlas (NanoString) (https://university.nanostring.com/geomx-ngs-pipeline-on-illumina-dragen-user-manual). Regions of interest (ROIs) were selected under immunofluorescence guidance to compare GREM1-high versus GREM1-low, HLA-DR-high versus HLA-DR-low, and PRG4-high versus PRG4-low regions. Sequencing data were processed using the GeoMx NGS pipeline. Differential expression analysis was performed using edgeR (v4.4.0) when ≤2 ROIs per group were available and DESeq2 (v1.46.0) otherwise. Genes with $|\log2FC| \geq 1$ and FDR < 0.05 were considered differentially expressed. Functional enrichment analysis was performed as described above.

Whole-mount immunostaining and three-dimensional reconstruction

Specimens were fixed in 4% paraformaldehyde (PFA) for 24 h and permeabilized through a graded methanol series. Samples were incubated with a primary antibody against HLA-DR (Abcam, ab92511) for 7 days, followed by incubation with a fluorophore-conjugated secondary antibody for 7 days. Tissues were cleared using an FDISCO solvent-based clearing kit (Jarvis Biotech) and imaged on a LiTone XL light-sheet microscope (Light Innovation Technology). Raw TIFF image stacks were stitched and processed using LitScan software and rendered in Imaris.

Cartilage organoid culture and stepwise ossification induction

Polydactyly-derived chondrocytes at passage 3 (P3) were used. Briefly, 2×10^5 cells were seeded per tube and cultured under a three-stage induction protocol. During days 1–7, organoids were maintained in high-glucose DMEM (H-DMEM) supplemented with 1× penicillin–streptomycin (P/S), 50 μg/ml ascorbic acid (VC), 10^{-7} M dexamethasone (DEX), 1% sodium pyruvate (SP), 1% Insulin-Transferrin-Selenium (ITS), and 10 ng/ml TGF-β3. During days 7–14, the medium was replaced with H-DMEM containing 10% fetal bovine serum (FBS), 1× P/S, 50 μg/ml VC, 10^{-8} M DEX, 5 ng/ml TGF-β3, and 100 ng/ml BMP2. During days 14–21, organoids were cultured

in H-DMEM supplemented with 10% FBS, 1× P/S, 50 μg/ml VC, 10^{-8} M DEX, 200 ng/ml BMP2, and 10 mM β-glycerophosphate. After induction, organoids were collected for embedding and sectioning, followed by alkaline phosphatase (ALP) staining (Beyotime) and HLA-DR immunostaining

Tissue processing and Safranin O/Fast Green staining Tissue samples were fixed in 4% paraformaldehyde for 24 h and decalcified in 10% EDTA. Samples were embedded in paraffin and sectioned at a thickness of 7 μm.

Sections were deparaffinized, rehydrated, and stained with hematoxylin, fast green, and safranin O for structural assessment. Images were acquired using a Pannoramic MIDI slide scanner (3DHISTECH).

Immunohistochemistry and immunofluorescence

For immunohistochemistry, tissue sections underwent antigen retrieval and blocking, followed by incubation with primary antibodies against CD31 (Huabio, M1511-8), ACTA2 (Huabio, ET1607-53), HBB (Santa Cruz Biotechnology, sc-21757), IGHM (Huabio, ET1702-81), TPSAB (Huabio, ET1610-64), and CD45 (Huabio, ET7111-03). HRP-conjugated secondary antibodies included goat anti-rabbit IgG (H+L) (Beyotime, A0208), goat anti-mouse IgG (H+L) (Beyotime, A0216), and goat anti-rat IgG (H+L) (Beyotime, A0192). Immunoreactivity was visualized using a DAB substrate kit (ZSGB-BIO). Whole-slide images were acquired using a Pannoramic MIDI slide scanner (3DHISTECH).

For immunofluorescence, tissue sections were incubated with primary antibodies against COL2 (Novus Biologicals, NB600-844), COL1 (Abcam, ab88147), GREM1 (Abcam, ab22138), CPXM1 (Invitrogen, PA5-31386), PDPN (Abcam, ab128994), HLA-DR (Abcam, ab92511), PTN (Novus Biologicals, MAB252-SP), PRG4 (Abcam, ab28484), POSTN (Huabio, ET1704-65), and OGN (Abcam, ab244329). Detection was performed using Alexa Fluor 555-conjugated goat anti-rabbit IgG H&L (Abcam, ab150078), Alexa Fluor 647-conjugated goat anti-mouse IgG H&L (Abcam, ab150115), or Alexa Fluor 647-conjugated donkey anti-rat IgG H&L (Abcam, ab150155), as appropriate. Nuclei were counterstained with DAPI. Images were acquired using an upright fluorescence microscope (Nikon, Japan).

Statistical analysis

Unless otherwise stated, experiments were performed with at least three independent samples per group. For comparisons between two groups, an unpaired two-tailed Student’s t-test was used for normally distributed data. Otherwise, the Mann–Whitney

U test was applied. Statistical analyses were conducted in GraphPad Prism (v10.2.0). A P value < 0.05 was considered statistically significant.

Author contributions

D.Y., Y.W. and J.C. contributed equally to this work. H.O. and Y.C. designed and supervised the study. J.C., W.W., B.W. and Y.W. collected human fetal and polydactyly tissue samples. Y.W. prepared polydactyly and cartilage organoid samples for single-cell RNA sequencing. D.Y. performed the GeoMx Digital Spatial Profiling (DSP) experiments with assistance from Y.Y. D.Y. and H.X. performed the histological and immunostaining experiments. D.Y. performed all single-cell and spatial transcriptomic analyses. Y.W. performed the in vitro cellular and molecular functional validation experiments. H.S., T.Q. and C.F. helped with data analysis. D.Y., Y.W. and Y.C. interpreted the results and wrote the manuscript. All authors discussed the results, revised the manuscript and approved the final version.

Acknowledgments

This work was supported by the National Key Research and Development Program of China (No. 2024YFA1108600), and the National Natural Sciences Foundation of China (T2121004, 82394441, 82622074, 82472457, 82502873).

Data availability

The single-cell RNA-sequencing and spatial transcriptomic datasets generated in this study have been deposited in National Genomics Data Center under accession number "HRA020521". Additional data supporting the findings of this study are available from the corresponding author upon reasonable request.

Reference

1 Mescher, A. L. in *Junqueira's Basic Histology: Text and Atlas, 18th Edition* (McGraw Hill, 2027).

2 Zhang, F. *et al.* An extra-erythrocyte role of haemoglobin body in chondrocyte hypoxia adaption. *Nature* **622**, 834-841 (2023). https://doi.org:10.1038/s41586-023-06611-6

3 Ramos, R. *et al.* Superstable lipid vacuoles endow cartilage with its shape and biomechanics. *Science* **387**, eads9960 (2025). https://doi.org:10.1126/science.ads9960

4 Ray, A., Singh, P. N., Sohaskey, M. L., Harland, R. M. & Bandyopadhyay, A. Precise spatial restriction of BMP signaling is essential for articular cartilage differentiation. *Development* **142**, 1169-1179 (2015). https://doi.org:10.1242/dev.110940

5 Darbellay, F. *et al.* Pre-hypertrophic chondrogenic enhancer landscape of limb and axial skeleton development. *Nat. Commun.* **15**, 4820 (2024). https://doi.org:10.1038/s41467-024-49203-2

6 Murphy, M. P. *et al.* Articular cartilage regeneration by activated skeletal stem cells. *Nat. Med.* **26**, 1583-1592 (2020). https://doi.org:10.1038/s41591-020-1013-2

7 Bai, L. *et al.* Engineering bone/cartilage organoids: strategy, progress, and application. *Bone Res.* **12**, 66 (2024). https://doi.org:10.1038/s41413-024-00376-y

8 Hartung, T. AI, agentic models and lab automation for scientific discovery - the beginning of scAInce. *Front Artif Intell* **8**, 1649155 (2025). https://doi.org:10.3389/frai.2025.1649155

9 Wenckstern, J. *et al.* The Virtual Tissues foundation model resolves spatial proteomics across scales. *Nature* **657**, 744-754 (2026). https://doi.org:10.1038/s41586-026-10884-y

10 Bunne, C. *et al.* How to build the virtual cell with artificial intelligence: Priorities and opportunities. *Cell* **187**, 7045-7063 (2024). https://doi.org:10.1016/j.cell.2024.11.015

11 O'Rahilly, R. & Gardner, E. The timing and sequence of events in the development of the limbs in the human embryo. *Anat. Embryol. (Berl.)* **148**, 1-23 (1975). https://doi.org:10.1007/BF00315559

12 Ben Hur, H. & Ornoy, A. Ultrastructural studies of initial stages of mineralization of long bones and vertebrae in human fetuses. *Acta Anat. (Basel)* **119**, 33-39 (1984). https://doi.org:10.1159/000145859

13 Zhang, B. *et al.* A human embryonic limb cell atlas resolved in space and time. *Nature* **635**, 668-678 (2024). https://doi.org:10.1038/s41586-023-06806-x

14 Merida-Velasco, J. A. *et al.* Development of the human knee joint. *Anat. Rec.* **248**, 269-278 (1997). https://doi.org:10.1002/(SICI)1097-0185(199706)248:2<269::AID-AR14>3.0.CO;2-N

15 Hita-Contreras, F. *et al.* Development of the human shoulder joint during the embryonic and early fetal stages: anatomical considerations for clinical practice. *J. Anat.* **232**, 422-430 (2018). https://doi.org:10.1111/joa.12753

16 To, K. *et al.* A multi-omic atlas of human embryonic skeletal development. *Nature* **635**, 657-667 (2024). https://doi.org:10.1038/s41586-024-08189-z

17 Ji, Q. *et al.* Single-cell RNA-seq analysis reveals the progression of human osteoarthritis. *Ann. Rheum. Dis.* **78**, 100-110 (2019). https://doi.org:10.1136/annrheumdis-2017-212863

18 J. Gordon Betts, K. A. Y., James A. Wise, Eddie Johnson, Brandon Poe, Dean H. Kruse, Oksana Korol, Jody E. Johnson, Mark Womble, Peter DeSaix. *Anatomy and Physiology 2e*. (OpenStax, 2022).

19 Noback, C. R. The developmental anatomy of the human osseous skeleton during the embryonic, fetal and circumnatal periods. *The Anatomical Record* **88**, 91-125 (1944). https://doi.org:https://doi.org/10.1002/ar.1090880107

20 Cavalli, E. *et al.* Characterization of polydactyly chondrocytes and their use in cartilage engineering. *Scientific Reports* **9**, 4275 (2019). https://doi.org:10.1038/s41598-019-40575-w

21 Kondo, M. *et al.* Safety and efficacy of human juvenile chondrocyte-derived cell sheets for osteochondral defect treatment. *npj Regenerative Medicine* **6**, 65 (2021). https://doi.org:10.1038/s41536-021-00173-9

22 He, J. *et al.* Dissecting human embryonic skeletal stem cell ontogeny by single-cell transcriptomic and functional analyses. *Cell Res.* **31**, 742-757 (2021). https://doi.org:10.1038/s41422-021-00467-z

23 Worthley, Daniel L. *et al.* Gremlin 1 Identifies a Skeletal Stem Cell with Bone, Cartilage, and Reticular Stromal Potential. *Cell* **160**, 269-284 (2015). https://doi.org:10.1016/j.cell.2014.11.042

24 Lei, Y., Xin, X., Morgan, D., Pintar, J. E. & Fricker, L. D. Identification of mouse CPX-1, a novel member of the metallocarboxypeptidase gene family with highest similarity to CPX-2. *DNA Cell Biol.* **18**, 175-185 (1999). https://doi.org:10.1089/104454999315565

25 Lanske, B. *et al.* PTH/PTHrP receptor in early development and Indian hedgehog-regulated bone growth. *Science* **273**, 663-666 (1996). https://doi.org:10.1126/science.273.5275.663

26 Yin, B. *et al.* Identification of Postn+ periosteal progenitor cells with bone regenerative potential. *JCI Insight* **9** (2024). https://doi.org:10.1172/jci.insight.182524

27 Zheng, Q. *et al.* Type X collagen gene regulation by Runx2 contributes directly to its hypertrophic chondrocyte-specific expression in vivo. *J. Cell Biol.* **162**, 833-842 (2003). https://doi.org:10.1083/jcb.200211089

28 Spath, S. S., Andrade, A. C., Chau, M., Baroncelli, M. & Nilsson, O. Evidence That Rat Chondrocytes Can Differentiate Into Perichondrial Cells. *JBMR Plus* **2**, 351-361 (2018). https://doi.org:10.1002/jbm4.10056

29 Delve, E., Co, V. & Kandel, R. A. Superficial and deep zone articular chondrocytes exhibit differences in actin polymerization status and actin-associated molecules in vitro. *Osteoarthr Cartil Open* **2**, 100071 (2020). https://doi.org:10.1016/j.ocarto.2020.100071

30 Roche, P. A. & Furuta, K. The ins and outs of MHC class II-mediated antigen processing and presentation. *Nat Rev Immunol* **15**, 203-216 (2015). https://doi.org:10.1038/nri3818

31 Didonna, A. *et al.* A splice acceptor variant in HLA-DRA affects the conformation and cellular localization of the class II DR alpha-chain. *Immunology* **162**, 194-207 (2021). https://doi.org:10.1111/imm.13273

32 Gao, M. *et al.* Deciphering postnatal limb development at single-cell resolution. *iScience* **26**, 105808 (2023). https://doi.org:10.1016/j.isci.2022.105808

33 Dobnikar, L. *et al.* Disease-relevant transcriptional signatures identified in individual smooth muscle cells from healthy mouse vessels. *Nat. Commun.* **9**, 4567 (2018). https://doi.org:10.1038/s41467-018-06891-x

34 Hadland, B. *et al.* Engineering a niche supporting hematopoietic stem cell development using integrated single-cell transcriptomics. *Nat. Commun.* **13**, 1584 (2022). https://doi.org:10.1038/s41467-022-28781-z

35 Korpetinou, A. *et al.* Serglycin: at the crossroad of inflammation and malignancy. *Front Oncol* **3**, 327 (2014). https://doi.org:10.3389/fonc.2013.00327

36 Schafflick, D. *et al.* Integrated single cell analysis of blood and cerebrospinal fluid leukocytes in multiple sclerosis. *Nat. Commun.* **11**, 247 (2020). https://doi.org:10.1038/s41467-019-14118-w

37 Jiang, J. *et al.* Gene signatures from scRNA-seq accurately quantify mast cells in biopsies in asthma. *Clin. Exp. Allergy* **50**, 1428-1431 (2020). https://doi.org:10.1111/cea.13732

38 Li, D. *et al.* Multidimensional profiling reveals GATA1-modulated stage-specific chromatin states and functional associations during human erythropoiesis. *Nucleic Acids Res.* **51**, 6634-6653 (2023). https://doi.org:10.1093/nar/gkad468

39 Walzer, S. M. *et al.* Vascularization of primary and secondary ossification centres in the human growth plate. *BMC Dev. Biol.* **14**, 36 (2014). https://doi.org:10.1186/s12861-014-0036-7

40 Pazzaglia, U. E. *et al.* Long bone human anlage longitudinal and circumferential growth in the fetal period and comparison with the growth plate cartilage of the postnatal age. *Microsc. Res. Tech.* **82**, 190-198 (2019). https://doi.org:10.1002/jemt.23153

41 JW, P. Time of ossification of the bones of the hand of the male and female and union of epiphyses with the diaphyses. *Am. J. Phys. Anthropol.* **8**, 401-410 (1925).

42 Gray, D. J., Gardner, E. & O'Rahilly, R. The prenatal development of the skeleton and joints of the human hand. *Am. J. Anat.* **101**, 169-223 (1957). https://doi.org:10.1002/aja.1001010202

43 Pazzaglia, U. E. *et al.* Relationship between the chondrocyte maturation cycle and the endochondral ossification in the diaphyseal and epiphyseal ossification centers. *J. Morphol.* **277**, 1187-1198 (2016). https://doi.org:10.1002/jmor.20568

44 Prokop-Piotrkowska, M., Marszalek-Dziuba, K., Moszczynska, E., Szalecki, M. & Jurkiewicz, E. Traditional and New Methods of Bone Age Assessment-An Overview. *J Clin Res Pediatr Endocrinol* **13**, 251-262 (2021). https://doi.org:10.4274/jcrpe.galenos.2020.2020.0091

45 Akiyama, H., Chaboissier, M. C., Martin, J. F., Schedl, A. & de Crombrugghe, B. The transcription factor Sox9 has essential roles in successive steps of the chondrocyte differentiation pathway and is required for expression of Sox5 and Sox6. *Genes Dev* **16**, 2813-2828 (2002). https://doi.org:10.1101/gad.1017802

46 Yang, Y. & Wilson, M. J. Lhx9 gene expression during early limb development in mice requires the FGF signalling pathway. *Gene Expr. Patterns* **19**, 45-51 (2015). https://doi.org:10.1016/j.gep.2015.07.002

47 Jachim, S. K. *et al.* Leveraging single cell multiomic analyses to identify gene regulatory networks that drive human articular cartilage cell fate. *Osteoarthritis Cartilage* **34**, 358-371 (2026). https://doi.org:10.1016/j.joca.2025.12.025

48 Im, S. & Kim, D. W. Nkx3.2 induces oxygen concentration-independent and lysosome-dependent degradation of HIF-1alpha to modulate hypoxic responses in chondrocytes. *Cell. Signal.* **36**, 127-138 (2017). https://doi.org:10.1016/j.cellsig.2017.05.001

49 Matsuzaki, T. *et al.* FoxO transcription factors modulate autophagy and proteoglycan 4 in cartilage homeostasis and osteoarthritis. *Sci. Transl. Med.* **10** (2018). https://doi.org:10.1126/scitranslmed.aan0746

50 Nagata, K. *et al.* Runx2 and Runx3 differentially regulate articular chondrocytes during surgically induced osteoarthritis development. *Nat. Commun.* **13**, 6187 (2022). https://doi.org:10.1038/s41467-022-33744-5

51 Chen, J. *et al.* DLX5 promotes Col10a1 expression and chondrocyte hypertrophy and is involved in osteoarthritis progression. *Genes Dis* **10**, 2097-2108 (2023). https://doi.org:10.1016/j.gendis.2022.12.016

52 Iwamoto, M., Golden, E. B., Adams, S. L., Noji, S. & Pacifici, M. Responsiveness to retinoic acid changes during chondrocyte maturation. *Exp. Cell Res.* **205**, 213-224 (1993). https://doi.org:10.1006/excr.1993.1079

53 Premnath, P., Zhu, Y., Besler, B. A., Boyd, S. & Krawetz, R. Overexpression of E2F1 in chondrocytes increases cartilaginous callus formation and consequent bone regeneration after fracture. *Osteoarthritis Cartilage* **26**, S91-S92 (2018). https://doi.org:10.1016/j.joca.2018.02.197

54 Chu, N. T. L. *et al.* A transcriptional atlas of the pubertal human growth plate reveals two populations of stem cells and direct effect of growth hormone. *Sci. Transl. Med.* **18**, eadw3590 (2026). https://doi.org:10.1126/scitranslmed.adw3590

55 Koziel, L., Wuelling, M., Schneider, S. & Vortkamp, A. Gli3 acts as a repressor downstream of Ihh in regulating two distinct steps of chondrocyte differentiation. *Development* **132**, 5249-5260 (2005). https://doi.org:10.1242/dev.02097

56 Iwamoto, M. *et al.* The role of ERG (ets related gene) in cartilage development. *Osteoarthritis Cartilage* **9 Suppl A**, S41-47 (2001). https://doi.org:10.1053/joca.2001.0443

57 Iwamoto, M. *et al.* Transcription factor ERG and joint and articular cartilage formation during mouse limb and spine skeletogenesis. *Dev Biol* **305**, 40-51 (2007). https://doi.org:10.1016/j.ydbio.2007.01.037

58 Zhu, N. *et al.* A Member of the Nuclear Receptor Superfamily, Designated as NR2F2, Supports the Self-Renewal Capacity and Pluripotency of Human Bone Marrow-Derived Mesenchymal Stem Cells. *Stem Cells Int* **2016**, 5687589 (2016). https://doi.org:10.1155/2016/5687589

59 Yang, J., Sun, W. & Cui, G. Roles of the NR2F Family in the Development, Disease, and Cancer of the Lung. *J Dev Biol* **12** (2024). https://doi.org:10.3390/jdb12030024

60 Jin, S. *et al.* Inference and analysis of cell-cell communication using CellChat. *Nat. Commun.* **12**, 1088 (2021). https://doi.org:10.1038/s41467-021-21246-9

61 Smith, C. W. *et al.* Recognition of an endothelial determinant for CD 18-dependent human neutrophil adherence and transendothelial migration. *J. Clin. Invest.* **82**, 1746-1756 (1988). https://doi.org:10.1172/JCI113788

62 Sui, X. F. *et al.* Receptor protein tyrosine phosphatase micro regulates the paracellular pathway in human lung microvascular endothelia. *Am. J. Pathol.* **166**, 1247-1258 (2005). https://doi.org:10.1016/s0002-9440(10)62343-7

63 Cheng, N., Brantley, D. M. & Chen, J. The ephrins and Eph receptors in angiogenesis. *Cytokine Growth Factor Rev* **13**, 75-85 (2002). https://doi.org:10.1016/s1359-6101(01)00031-4

64 Worthley, D. L. *et al.* Gremlin 1 identifies a skeletal stem cell with bone, cartilage, and reticular stromal potential. *Cell* **160**, 269-284 (2015). https://doi.org:10.1016/j.cell.2014.11.042

65 Ng, J. Q. *et al.* Loss of Grem1-lineage chondrogenic progenitor cells causes osteoarthritis. *Nat. Commun.* **14**, 6909 (2023). https://doi.org:10.1038/s41467-023-42199-1

66 Merino, R. *et al.* The BMP antagonist Gremlin regulates outgrowth, chondrogenesis and programmed cell death in the developing limb. *Development* **126**, 5515-5522 (1999). https://doi.org:10.1242/dev.126.23.5515

67 Lancman, J. J. *et al.* Downregulation of Grem1 expression in the distal limb mesoderm is a necessary precondition for phalanx development. *Dev. Dyn.* **251**, 1439-1455 (2022). https://doi.org:10.1002/dvdy.431

68 Hu, K., Sun, H., Gui, B. & Sui, C. Gremlin-1 suppression increases BMP-2-induced osteogenesis of human mesenchymal stem cells. *Mol Med Rep* **15**, 2186-2194 (2017). https://doi.org:10.3892/mmr.2017.6253

69 Leijten, J. C. *et al.* Gremlin 1, frizzled-related protein, and Dkk-1 are key regulators of human articular cartilage homeostasis. *Arthritis Rheum* **64**, 3302-3312 (2012). https://doi.org:10.1002/art.34535

70 Ignatyeva, N., Gavrilov, N., Timashev, P. S. & Medvedeva, E. V. Prg4-Expressing Chondroprogenitor Cells in the Superficial Zone of Articular Cartilage. *Int. J. Mol. Sci.* **25** (2024). https://doi.org:10.3390/ijms25115605

71 Xuan, F. *et al.* Wnt/beta-catenin signaling contributes to articular cartilage homeostasis through lubricin induction in the superficial zone. *Arthritis Res. Ther.* **21**, 247 (2019). https://doi.org:10.1186/s13075-019-2041-5

72 Ji, Y. *et al.* CD99 promotes self-renewal in hematopoietic stem cells and leukemia stem cells by regulating protein synthesis. *Blood* **146**, 1914-1928 (2025). https://doi.org:10.1182/blood.2024026271

73 Gigout, A. *et al.* Chondrocyte aggregation in suspension culture is GFOGER-GPP- and beta1 integrin-dependent. *J. Biol. Chem.* **283**, 31522-31530 (2008). https://doi.org:10.1074/jbc.M804234200

74 Duchamp de Lageneste, O. *et al.* Periosteum contains skeletal stem cells with high bone regenerative potential controlled by Periostin. *Nat. Commun.* **9**, 773 (2018). https://doi.org:10.1038/s41467-018-03124-z

75 Zhao, L. *et al.* Single-cell mapping reveals age-related alterations in periosteal progenitor cells and immune microenvironment. *Cell Regen* **14**, 46 (2025). https://doi.org:10.1186/s13619-025-00263-9

76 Notoh, H. *et al.* Spatiotemporal dynamics and ossification of podoplanin-positive cells in the developing femur. *Sci Rep* **16** (2026). https://doi.org:10.1038/s41598-026-46913-z

77 Liu, S. *et al.* Monocytic HLA-DR Expression in Immune Responses of Acute Pancreatitis and COVID-19. *Int. J. Mol. Sci.* **24** (2023). https://doi.org:10.3390/ijms24043246

78 Lance, E. M., Kimura, L. H. & Manibog, C. N. The expression of major histocompatibility antigens on human articular chondrocytes. *Clin. Orthop. Relat. Res.*, 266-282 (1993).

79 Pishesha, N., Harmand, T. J. & Ploegh, H. L. A guide to antigen processing and presentation. *Nat Rev Immunol* **22**, 751-764 (2022). https://doi.org:10.1038/s41577-022-00707-2

80 Stickens, D. *et al.* Altered endochondral bone development in matrix metalloproteinase 13-deficient mice. *Development* **131**, 5883-5895 (2004). https://doi.org:10.1242/dev.01461

81 Yi, J. *et al.* Elastin-derived extracellular matrix fragments drive aging through innate immune activation. *Nature Aging* **5**, 2380-2398 (2025). https://doi.org:10.1038/s43587-025-00961-8

82 Bouderlique, T. *et al.* Pleiotrophin commits human bone marrow mesenchymal stromal cells towards hypertrophy during chondrogenesis. *PLoS ONE* **9**, e88287 (2014). https://doi.org:10.1371/journal.pone.0088287

83 Zhang, Y. *et al.* Mapping the trajectory of organoid research: Insights into complex models and advanced technologies. *Engineered Regeneration* **6**, 264-276 (2025). https://doi.org:https://doi.org/10.1016/j.engreg.2025.11.003

84 Li, S. *et al.* Microenvironment-responsive nanosystems for osteoarthritis therapy. *Engineered Regeneration* **5**, 92-110 (2024). https://doi.org:https://doi.org/10.1016/j.engreg.2023.12.002

85 Wen, Y. *et al.* Hyperplastic Human Macromass Cartilage for Joint Regeneration. *Adv Sci (Weinh)* **10**, e2301833 (2023). https://doi.org:10.1002/advs.202301833

86 Won, Y. *et al.* Pleiotropic roles of metallothioneins as regulators of chondrocyte apoptosis and catabolic and anabolic pathways during osteoarthritis pathogenesis. *Ann. Rheum. Dis.* **75**, 2045-2052 (2016). https://doi.org:10.1136/annrheumdis-2015-208406

87 Lim, C. L. *et al.* Immunogenicity and immunomodulatory effects of the human chondrocytes, hChonJ. *BMC Musculoskelet Disord* **18**, 199 (2017). https://doi.org:10.1186/s12891-017-1547-8

88 He, J. *et al.* Dissecting human embryonic skeletal stem cell ontogeny by single-cell transcriptomic and functional analyses. *Cell Res.* **31**, 742-757 (2021). https://doi.org:10.1038/s41422-021-00467-z

89 Yamada, D. *et al.* Induction and expansion of human PRRX1+ limb-bud-like mesenchymal cells from pluripotent stem cells. *Nature Biomedical Engineering* **5**, 926-940 (2021). https://doi.org:10.1038/s41551-021-00778-x

90 Dominici, M. *et al.* Minimal criteria for defining multipotent mesenchymal stromal cells. The International Society for Cellular Therapy position statement. *Cytotherapy* **8**, 315-317 (2006). https://doi.org:10.1080/14653240600855905

91 Yamada, D. *et al.* Identification of Surface Antigens That Define Human Pluripotent Stem Cell-Derived PRRX1+Limb-Bud-like Mesenchymal Cells. *Int. J. Mol. Sci.* **23** (2022). https://doi.org:10.3390/ijms23052661

92 Petibon, C., Malik Ghulam, M., Catala, M. & Abou Elela, S. Regulation of ribosomal protein genes: An ordered anarchy. *Wiley Interdiscip Rev RNA* **12**, e1632 (2021). https://doi.org:10.1002/wrna.1632

93 Lau, L. F. CCN1/CYR61: the very model of a modern matricellular protein. *Cell. Mol. Life Sci.* **68**, 3149-3163 (2011). https://doi.org:10.1007/s00018-011-0778-3

94 Johansen, J. S., Hoyer, P. E., Larsen, L. A., Price, P. A. & Mollgard, K. YKL-40 protein expression in the early developing human musculoskeletal system. *J. Histochem. Cytochem.* **55**, 1213-1228 (2007). https://doi.org:10.1369/jhc.7A7245.2007

95 Jiang, H. *et al.* LncRNA SNHG5 promotes chondrocyte proliferation and inhibits apoptosis in osteoarthritis by regulating miR-10a-5p/H3F3B axis. *Connect. Tissue Res.* **62**, 605-614 (2021). https://doi.org:10.1080/03008207.2020.1825701

96 Rikkers, M., Korpershoek, J. V., Levato, R., Malda, J. & Vonk, L. A. Progenitor Cells in Healthy and Osteoarthritic Human Cartilage Have Extensive Culture Expansion Capacity while Retaining Chondrogenic Properties. *Cartilage* **13**, 129S-142S (2021). https://doi.org:10.1177/19476035211059600

97 Hao, Y. *et al.* Integrated analysis of multimodal single-cell data. *Cell* **184**, 3573-3587 e3529 (2021). https://doi.org:10.1016/j.cell.2021.04.048

98 McGinnis, C. S., Murrow, L. M. & Gartner, Z. J. DoubletFinder: Doublet Detection in Single-Cell RNA Sequencing Data Using Artificial Nearest Neighbors. *Cell Systems* **8**, 329-337.e324 (2019). https://doi.org:10.1016/j.cels.2019.03.003

99 Heaton, H. *et al.* Souporcell: robust clustering of single-cell RNA-seq data by genotype without reference genotypes. *Nature Methods* **17**, 615-620 (2020). https://doi.org:10.1038/s41592-020-0820-1

100 Efremova, M., Vento-Tormo, M., Teichmann, S. A. & Vento-Tormo, R. CellPhoneDB: inferring cell–cell communication from combined expression of multi-subunit ligand–receptor complexes. *Nat. Protoc.* **15**, 1484-1506 (2020). https://doi.org:10.1038/s41596-020-0292-x

101 Jin, S. *et al.* Inference and analysis of cell-cell communication using CellChat. *Nat. Commun.* **12**, 1088 (2021). https://doi.org:10.1038/s41467-021-21246-9

102 Cao, J. *et al.* The single-cell transcriptional landscape of mammalian organogenesis. *Nature* **566**, 496-502 (2019). https://doi.org:10.1038/s41586-019-0969-x

103 La Manno, G. *et al.* RNA velocity of single cells. *Nature* **560**, 494-498 (2018). https://doi.org:10.1038/s41586-018-0414-6

104 Bergen, V., Lange, M., Peidli, S., Wolf, F. A. & Theis, F. J. Generalizing RNA velocity to transient cell states through dynamical modeling. *Nat. Biotechnol.* **38**, 1408-1414 (2020). https://doi.org:10.1038/s41587-020-0591-3

105 Aibar, S. *et al.* SCENIC: single-cell regulatory network inference and clustering. *Nature Methods* **14**, 1083-1086 (2017). https://doi.org:10.1038/nmeth.4463

106 Lopez, R., Regier, J., Cole, M. B., Jordan, M. I. & Yosef, N. Deep generative modeling for single-cell transcriptomics. *Nat. Methods* **15**, 1053-1058 (2018). https://doi.org:10.1038/s41592-018-0229-2

107 Polanski, K. *et al.* BBKNN: fast batch alignment of single cell transcriptomes. *Bioinformatics* **36**, 964-965 (2020). https://doi.org:10.1093/bioinformatics/btz625

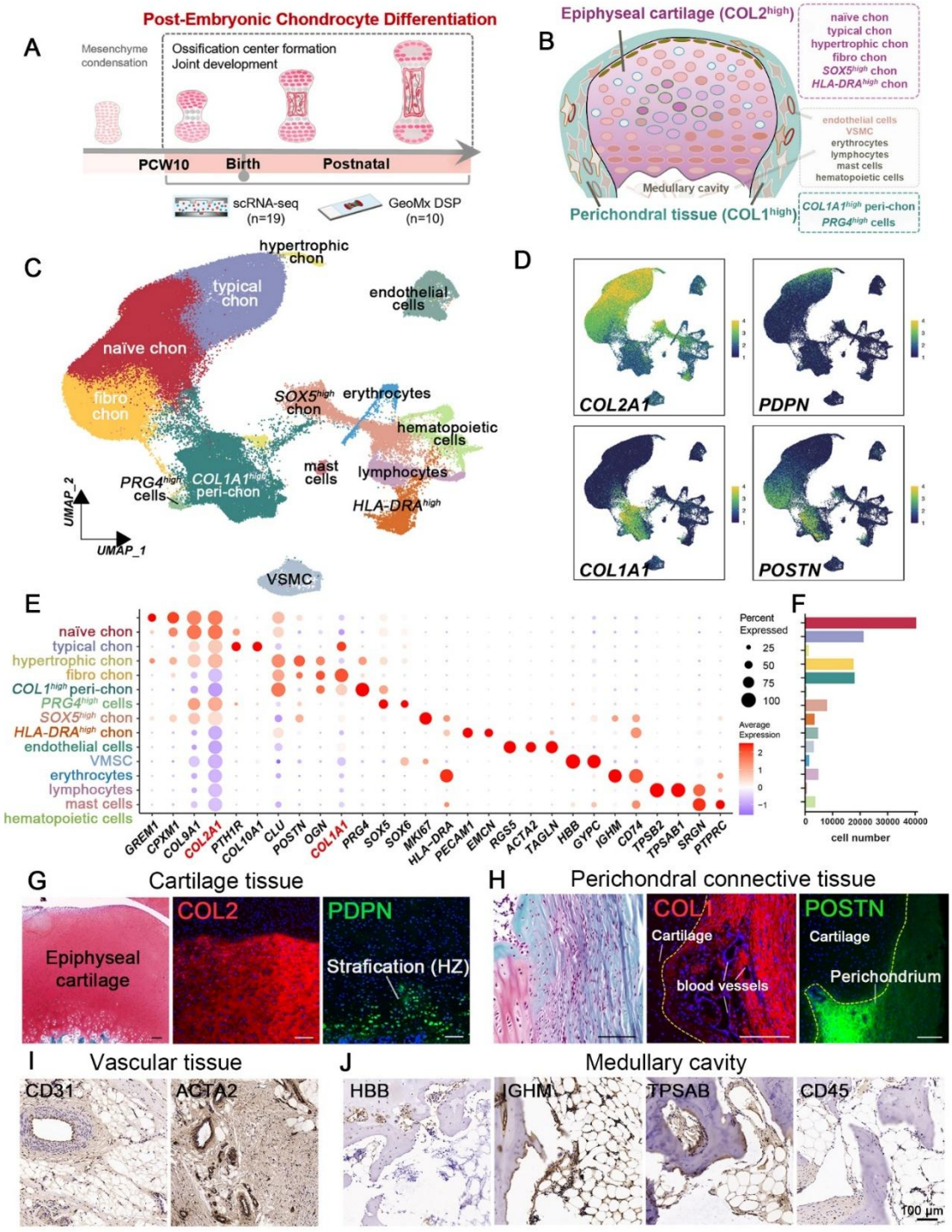


Figure 1. Cellular diversity in post-embryonic human digits.

(A) Schematic overview of sample collection and the experimental workflow for single-cell RNA sequencing (scRNA-seq) and GeoMx digital spatial profiling (DSP). (B) Schematic of digit cartilage anatomy and the spatial distribution of major cell populations. (C) Uniform Manifold Approximation and Projection (UMAP) of cell clusters identified in post-embryonic human digit samples. (D) UMAP feature plots of representative lineage markers, including *COL2A1*, *PDPN*, *COL1A1* and *POSTN*. (E) Dot plot of canonical marker genes used for cell type annotation. Dot size indicates the percentage of cells expressing each gene and color indicates average expression. (F) Bar plot showing cell numbers of the

14 annotated cell populations. (G) Safranin O/Fast Green staining of cartilage, with corresponding immunofluorescence staining for COL2 and PDPN. (H) Safranin O/Fast Green staining of perichondral connective tissue, with corresponding immunofluorescence staining for COL1 and POSTN. (I) Immunohistochemical staining for CD31 and ACTA2 in vascular tissue. (J) Immunohistochemical staining for HBB, IGHM, TPSAB and CD45 in the medullary cavity. Scale bars, 100 μm (G-J).

Abbreviations: naïve chon, *GREM1*^{high} naïve chondrocytes; typical chon, *COL9A1*^{high} *GREM1*^{low} typical chondrocytes; hypertrophic chon, *PTH1R*^{high} hypertrophic chondrocytes; fibro chon, *COL9A1*^{high} *POSTN*^{high} fibrochondrocytes; *COL1A1*^{high} peri-chon, *COL1A1*^{high} perichondral cells; *SOX5*^{high} chon, *SOX5*^{high} *SOX6*^{high} chondrocytes; *HLA-DRA*^{high} chon, *HLA-DRA*^{high} chondrocytes; VSMC, vascular smooth muscle cells.

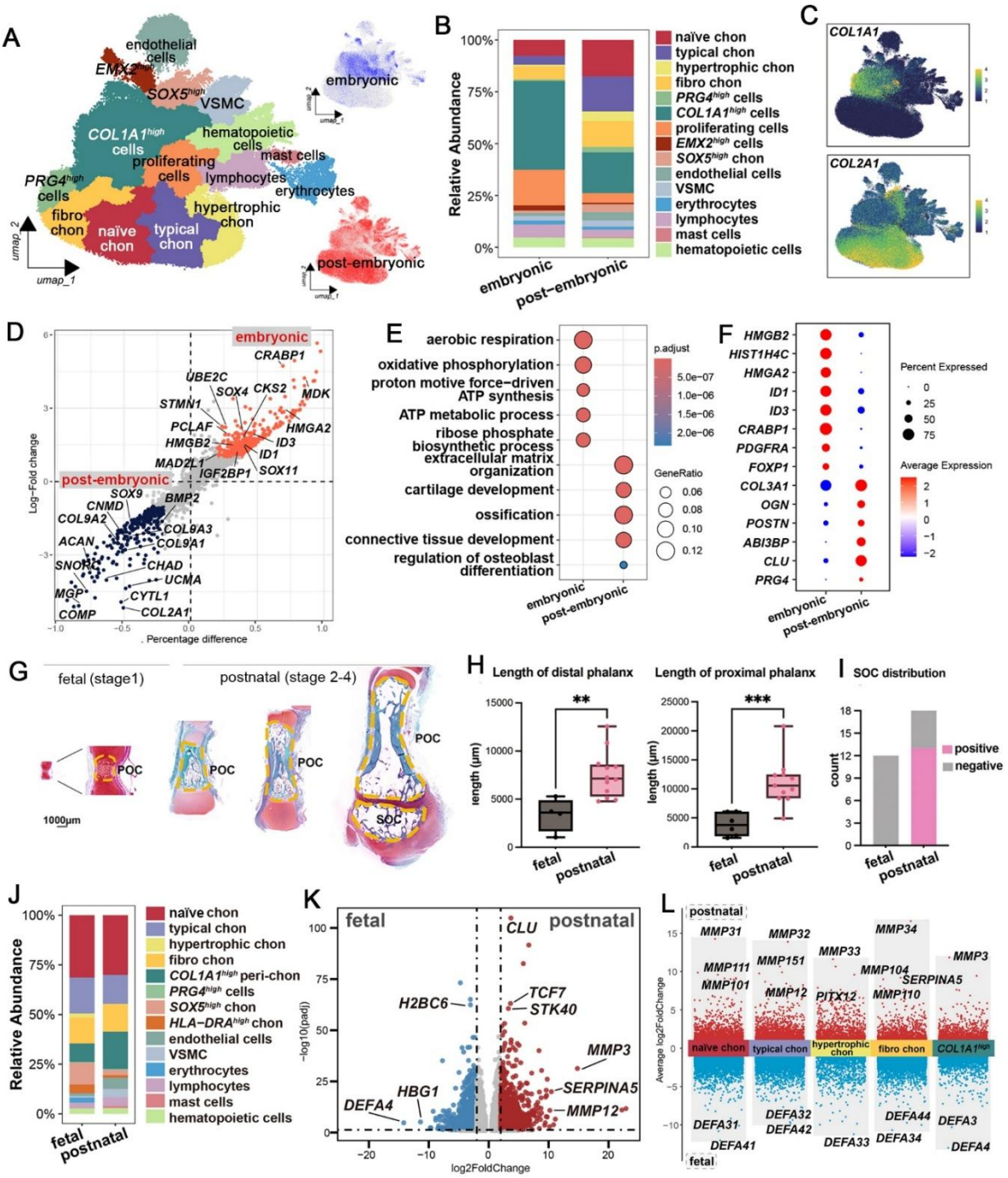


Figure 2. Emergence of *COL2A1*^{high} chondrocytes and niche remodeling programs in post-embryonic stages.

(A) UMAP of integrated embryonic limb and post-embryonic digit datasets (left), with embryonic and post-embryonic cells highlighted separately in the same embedding (right). (B) Stacked bar plot showing the proportions of cell populations in embryonic and post-embryonic samples. (C) UMAP feature plots of *COL1A1* and *COL2A1* expression. (D) Volcano plot of differentially expressed genes between embryonic and post-embryonic samples. (E) Gene Ontology (GO) Biological Process enrichment analysis of genes upregulated in embryonic or post-embryonic samples. (F) Dot plot of selected genes associated with proliferation, progenitor states and fibrosis in *COL1A1*^{high} cells from

embryonic and post-embryonic samples. (G) Safranin O/Fast Green staining across four histologically defined stages of post-embryonic digit maturation. Scale bar, 1 mm. (H) Comparison of distal and proximal phalanx lengths between fetal and postnatal specimens. Distal phalanx: n = 4 fetal and 12 postnatal specimens, $P = 0.0069$; proximal phalanx: n = 6 fetal and 11 postnatal specimens, $P = 0.0009$; unpaired two-tailed Student's *t*-test. (I) Counts of fetal and postnatal specimens with or without secondary ossification centers (SOCs). (J) Stacked bar plot of cell-subpopulation proportions in fetal and postnatal samples. (K) Volcano plot of differentially expressed genes between postnatal and fetal samples. (L) Volcano plot of differentially expressed genes within individual chondrocyte subpopulations between postnatal and fetal samples.

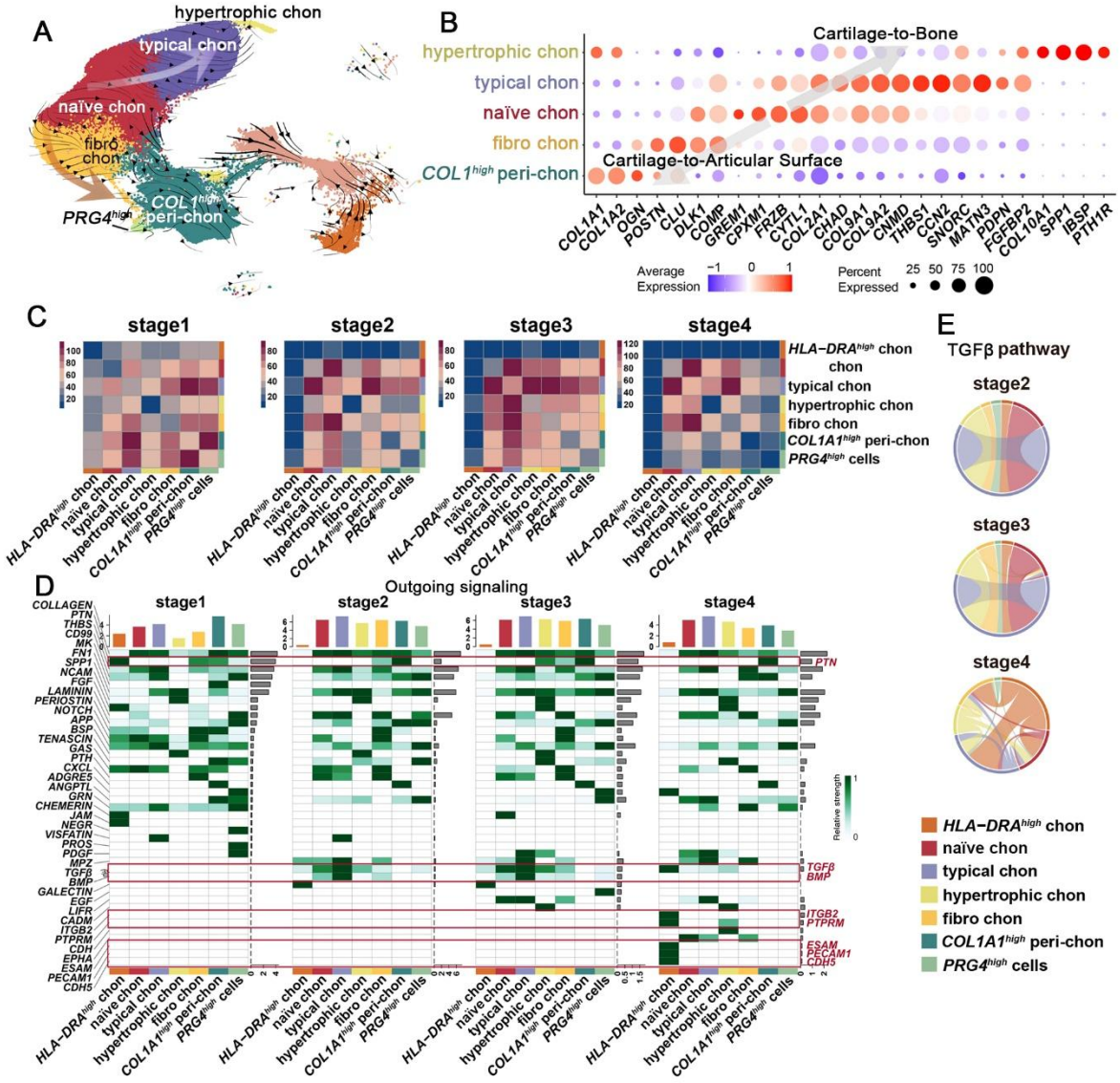


Figure 3. Dynamical programs of chondrocyte fate commitment and niche crosstalk.

(A) RNA velocity analysis of cartilage-associated subpopulations, showing inferred cell-state transitions. (B) Dot plot of marker-gene expression across cartilage-associated subpopulations. (C) Stage-resolved intercellular communication strength among cartilage-associated subpopulations. (D) Outgoing signaling patterns of cartilage-associated subpopulations across four developmental stages. (E) Chord diagrams showing tissue growth factor beta (TGFβ) signaling among cartilage-associated subpopulations across developmental stages.

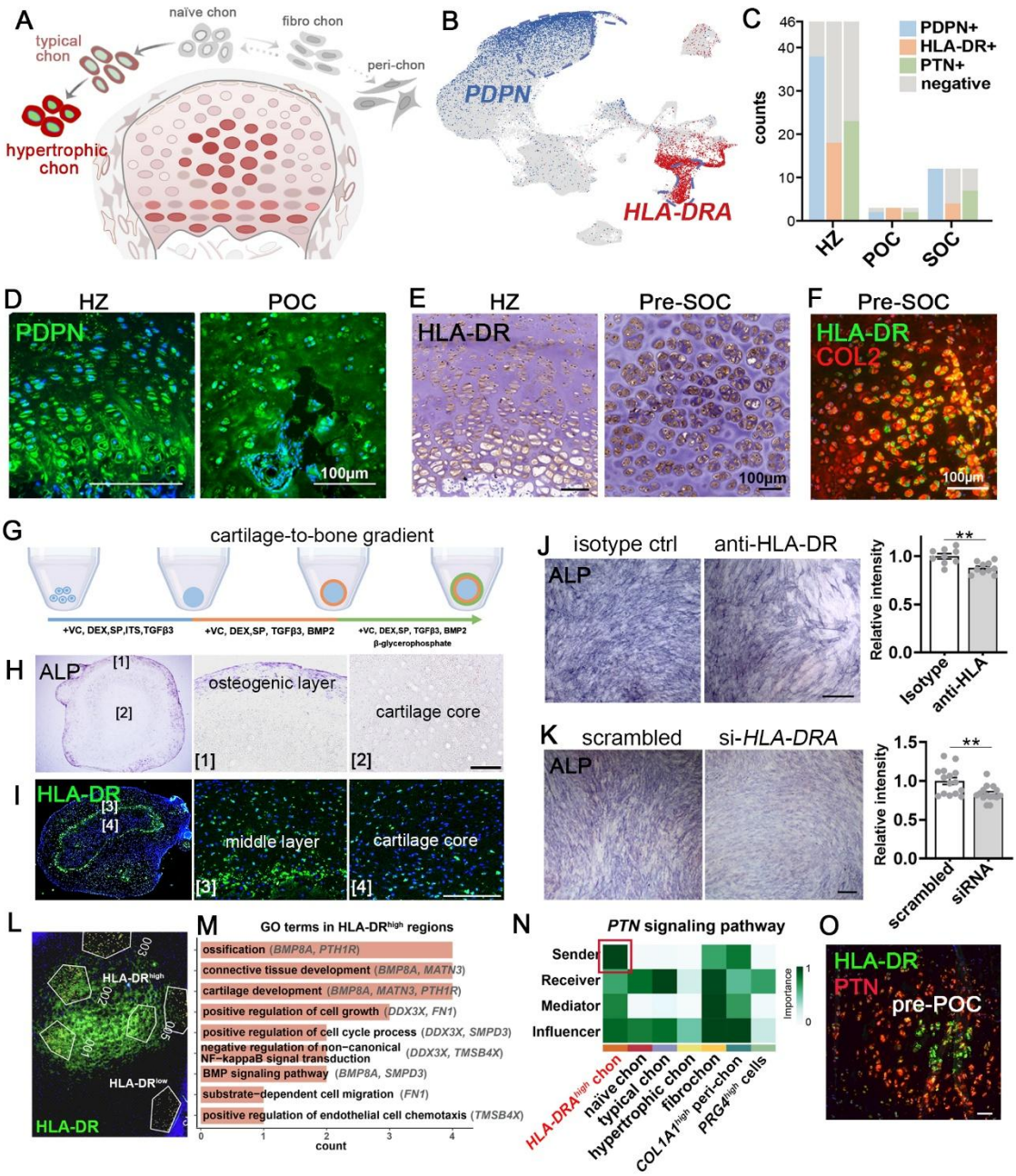


Figure 4. Discovery of *HLA-DRA*^{high} chon, a new chondrocyte subpopulation with early ossified phenotype.

(A) Schematic of the inferred osteochondral differentiation trajectory and the spatial localization of *HLA-DRA*^{high} chondrocytes within the digit cartilage. (B) UMAP feature plot of *PDPN* and *HLA-DRA* expression. (C) Quantification of immunohistochemical signals for PTN, HLA-DR, and PDPN across the calcified hypertrophic zone, primary ossification center (POC) and secondary ossification center (SOC). (D) Immunofluorescence staining for PDPN in the hypertrophic zone and POC. (E) Immunohistochemical staining for HLA-DR in the hypertrophic zone and pre-SOC region. (F) Immunofluorescence co-staining for COL2 and HLA-DR in the pre-SOC region. (G) Schematic of the in vitro chondrocyte osteogenic induction model and experimental workflow. (H) Alkaline phosphatase (ALP) staining following osteogenic induction. (I) Immunofluorescence staining for

HLA-DR following osteogenic induction. (J) ALP staining and relative staining intensity following treatment with an isotype control antibody or anti-HLA-DR antibody during osteogenic induction. (K) ALP staining and relative staining intensity following transfection with scrambled siRNA or *HLA-DRA*-targeting siRNA during osteogenic induction. (L) Immunofluorescence-guided selection of HLA-DR^{high} and HLA-DR^{low} regions of interest (ROIs) for GeoMx DSP. (M) Gene Ontology (GO) Biological Process enrichment analysis of genes enriched in HLA-DR^{high} ROIs. (N) Heatmap of PTN signaling activity among chondrocyte subpopulations. (O) Immunofluorescence staining showing spatial overlap between PTN and HLA-DR in pre-POC region. Scale bars, 100 μm (D–F, H–K, O).

Abbreviations: VC, ascorbic acid; DEX, dexamethasone; SP, sodium pyruvate; ITS, insulin–transferrin–selenium.

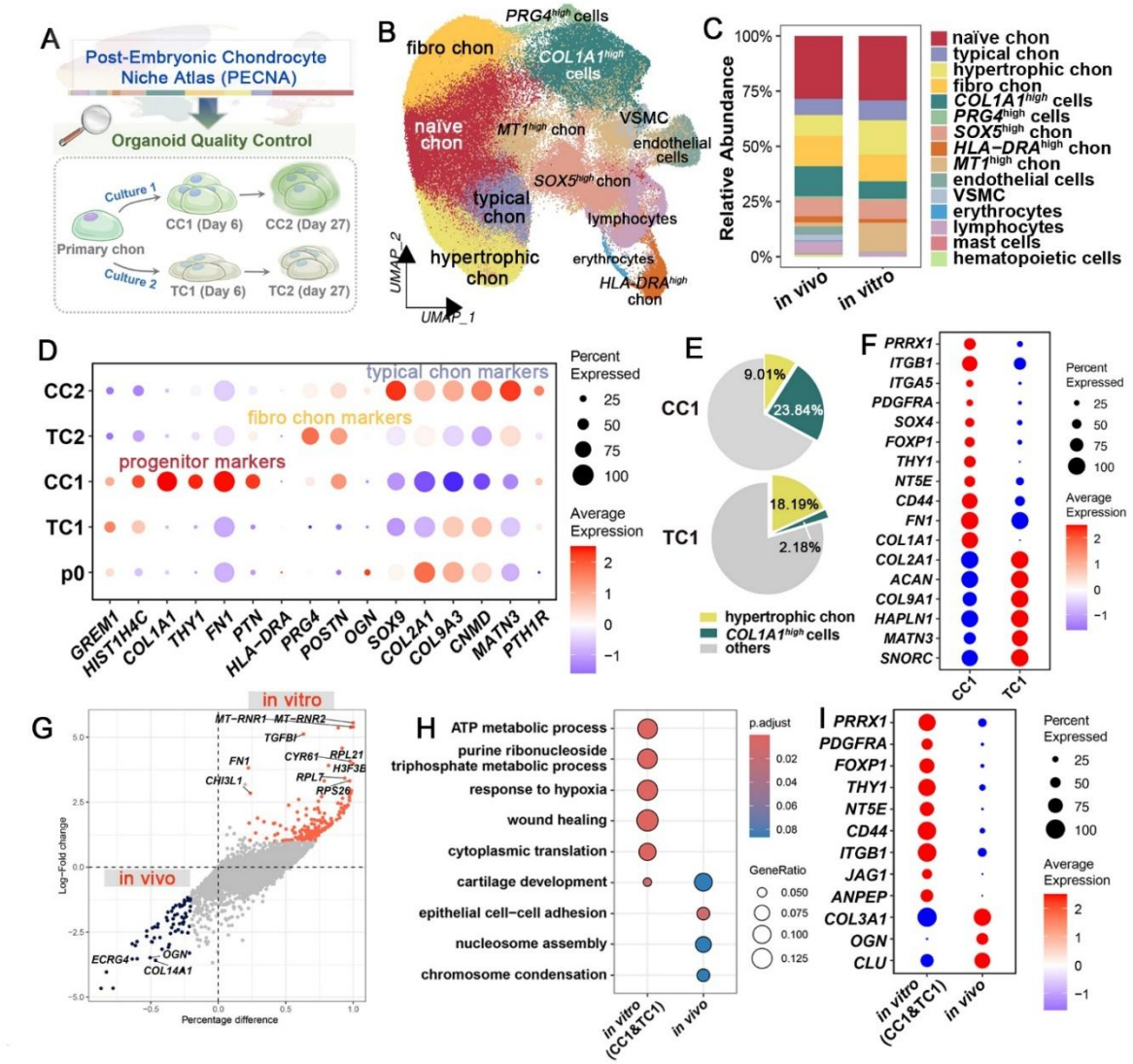


Figure 5. The digital Post-Embryonic Chondrocyte Niche Atlas (PECNA), a reference to guide organoid engineering

(A) Schematic overview of the comparison between in vitro chondrocyte microtissues and PECNA as an in vivo reference, with the sampling time points and culture conditions of the in vitro dataset. Primary chondrocytes (P0) were cultured under customized conditions (CC) or typical conditions (TC) and collected on day 6 (CC1 and TC1) and day 27 (CC2 and TC2). (B) UMAP of the integrated in vivo and in vitro single-cell datasets. (C) Stacked bar plot showing cell-type proportions across in vivo and in vitro samples. (D) Dot plot of selected developmental genes from the in vivo reference across in vitro culture stages and conditions. (E) Pie charts showing cell-type proportions in TC1 and CC1. (F) Dot plot of stem/progenitor-associated genes and canonical cartilage markers in CC1 and TC1. (G) Volcano plot of differentially expressed genes between in vitro *COL1A1*^{high} cells from the proliferation stage (CC1 and TC1) and in vivo *COL1A1*^{high} cells. (H) Gene Ontology (GO) Biological Process enrichment analysis of differentially expressed genes identified in **G**. (I) Dot plot of selected differentially expressed genes in *COL1A1*^{high} cells across in vivo and in vitro conditions.

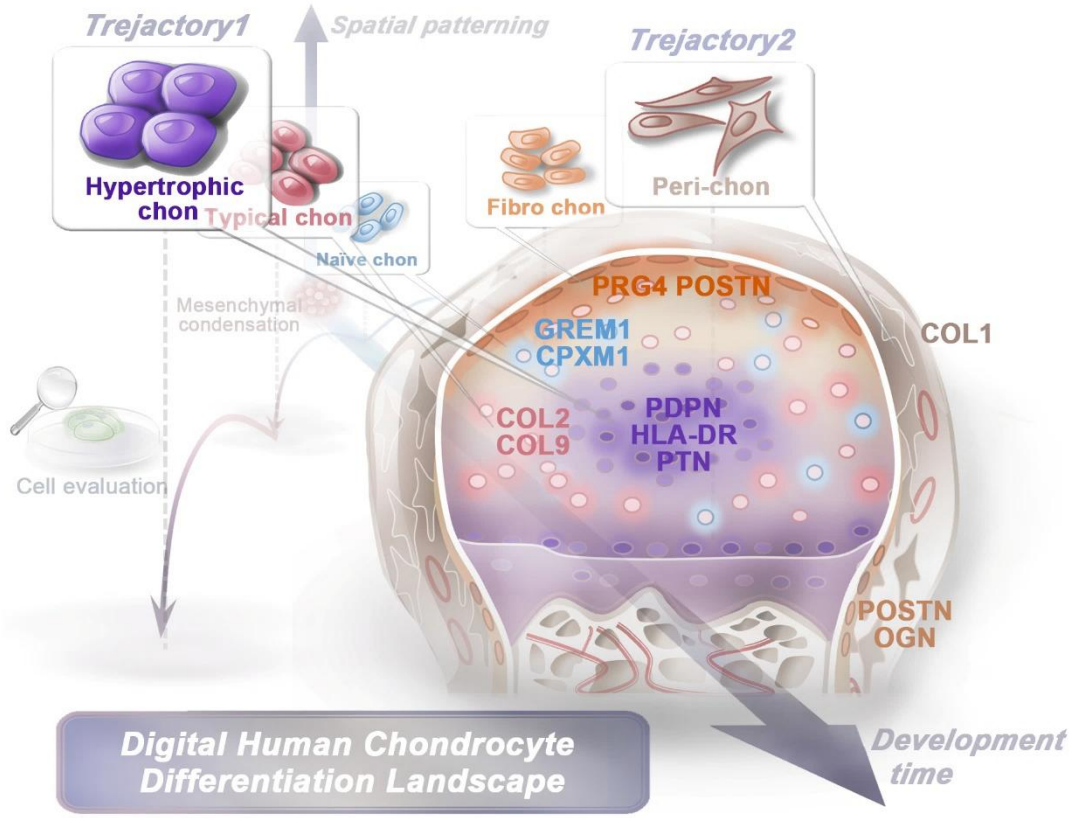


Figure 6. A landscape of human post-embryonic chondrocyte differentiation reveals chondrocyte fate trajectories and provides a reference for engineered-cartilage evaluation

This atlas delineates molecularly distinct chondrocyte subpopulations with characteristic spatial localization and two major developmental fate trajectories toward articular differentiation and endochondral ossification within human post-embryonic digits. Serving as an in-vivo developmental reference, it informs the studies of cartilage development and supports the optimization of chondrocyte-based regenerative therapies.

Supplementary Files

This is a list of supplementary files associated with this preprint. Click to download.

- supplementarymaterials.docx
- SupplementaryTable6.DifferentiallyexpressedmarkergenesforcellpopulationsidentifiedbysinglecellRNAsequencing.xlsx